2019-08-23

Rupture geometries in anisotropic amphibolite recorded by pseudotachylytes in the Gairloch Shear Zone, NW Scotland

Campbell, LR

10.1144/sjg2019-003
Scottish Journal of Geology
Geological Society

Rupture geometries in anisotropic amphibolite recorded by pseudotachylytes in the Gairloch Shear Zone, NW Scotland

Lucy R. Campbell[1,2*], Richard J. Phillips[1], Rachel C. Walcott[3] & Geoffrey E. Lloyd[1]

[1] School of Earth and Environment, University of Leeds, LS2 9JT, UK

[2]Present address: School of Geography, Earth and Environmental Sciences, Plymouth University, PL4 8AA, UK.

[3] National Museums Scotland, Chambers Street. Edinburgh, EH1 1JF, UK

*Corresponding author (email: lucy.campbell@plymouth.ac.uk)

Abstract

Recent earthquakes involving complex multi-fault rupture have increased our appreciation of the variety of rupture geometries and fault interactions that occur within the short duration of coseismic slip. Geometrical complexities are intrinsically linked with spatially heterogeneous slip and stress drop distributions, and hence need incorporating into seismic hazard analysis. Studies of exhumed ancient fault zones facilitate investigation of rupture processes in the context of lithology and structure at seismogenic depths. In the Gairloch Shear Zone, NW Scotland, foliated amphibolites host pseudotachylytes that record rupture geometries of ancient low-magnitude (≤ M_W 3) seismicity. Pseudotachylyte faults are commonly foliation parallel, indicating exploitation of foliation planes as weak interfaces for seismic rupture. Discordance and complexity are introduced by fault segmentation, stepovers, branching and brecciated dilational volumes. Pseudotachylyte geometries indicate that slip nucleation initiated simultaneously across several parallel foliation planes with millimetre and centimetre separations, leading to progressive interaction and ultimately linkage of adjacent segments and branches within a single earthquake. Interacting with this structural control, a lithological influence of abundant low disequilibrium melting-point amphibole facilitated coseismic melting, with relatively high coseismic melt pressure encouraging transient dilational sites. These faults elucidate controls and processes that may upscale to large active fault zones hosting major earthquake activity.

Supplementary material: Supplementary Figures 1 and 2, unannotated versions of field photographs displayed in Figures 4a and 5 respectively, are available at

Seismic hazard mapping depends heavily on understanding the geometry of fault planes and earthquake rupture, which are best understood from examination of surface ruptures and analogous exhumed fault zones. Recent earthquakes have widened understanding of the possible complexities of rupture, allowing the creation of many alternative models to a simple single planar fault, for example the multi-segment 2016 M_W 7.8 Kaikōura earthquake (Hamling *et al*. 2017), the 2018 M_W 7.9 offshore Kodiak earthquake (Ruppert *et al.* 2018) and the 2010 M_W 7.2 El-Mayor-Cucapah earthquake (Fletcher *et al.* 2016). The potential for multi-segment rupture is, however, not typically accounted for in seismic hazard modelling (Nissen *et al.* 2016). Supporting this new understanding is a body of research characterising the geometry and development of exhumed fault zones, which reveal greater complexity at scales typically less than the resolution of seismological records (e.g. Sibson 1975, Swanson, 1988, Allen et al., 2002, Di Toro & Pennacchioni 2005, Rowe et al., 2018). Significantly, exhumed faults reveal geometries and deformation mechanisms of faults at seismogenic depths (e.g. Sibson 1975; Swanson 1988; Allen *et al.* 2002; Di Toro and Pennacchioni 2005; Ujiie *et al.* 2007; Griffith et al. 2010; Rowe *et al.* 2011, 2018; Kirkpatrick *et al.* 2012; Ferrand *et al.* 2018).

Pseudotachylyte, a melt-derived fault rock produced during coseismic frictional heating (Sibson 1975), remains one of the best recognised markers of ancient seismicity (Cowan 1999; Rowe & Griffith 2015). It has been extensively utilised to study seismic source parameters and rupture geometries from exhumed fault zones worldwide and across a range of depths (e.g. Sibson 1975; Swanson 1988; Allen *et al.* 2002; Di Toro and Pennacchioni 2005; Ujiie *et al.* 2007; Griffith et al. 2010; Rowe *et al.* 2011, 2018; Kirkpatrick *et al.* 2012; Ferrand *et al.* 2018). Pseudotachylyte–bearing faults illustrate a variety of fault plane and damage zone geometries, including the melt-generating fault planes, tensile off-fault injection veins, chaotic networks of off-fault veining, and dilational sites often hosting breccias, all of which may illustrate the heterogeneous and dynamic environment of coseismic rupture (Sibson 1975, 1985; Swanson 2005; Kirkpatrick & Shipton 2009; Ngo *et al.* 2012; Griffith & Prakash 2015; Rowe *et al*. 2018).

In the context of successive frictional failure, pseudotachylytes are frequently inferred to weld fault planes once they have cooled, such that later brittle slip events rarely reactivate unaltered pseudotachylyte-bearing faults (Mitchell *et al*. 2016, Phillips et al., 2019). Consequentially, a suite of pseudotachylyte faults may preserve snapshots of seismic rupture evolution that have evaded reactivation and/or destruction by later slip events along the same fault plane, although they may be subject to subsequent recrystallization, viscous deformation and mineralogical alteration (Kirkpatrick & Rowe 2013, Phillips et al., 2019). In the Gairloch Shear Zone (GSZ), NW Scotland, well-preserved 1019-910 Ma pseudotachylytes potentially record brittle Renlandian deformation (950-940 Ma) that exploited the fabric of pre-existing Laxfordian (1800-1500 Ma) ductile shear zones, although work pre-dating the recognition of the Renlandian event in northwest Scotland (Bird et al., 2018) tends to infer earlier Grenvillian (~1100 Ma) related deformation for brittle GSZ faults (Lei & Park 1993; Sherlock *et al.* 2008). The pseudotachylytes record foliation-parallel seismic rupture in a variety of fault plane and damage zone geometries including stepping fault segments, dilational pull-aparts, branching faults and breccias (e.g. Park 1961). However, the context of the ancient seismicity that they record has not so far been comprehensively investigated.

In this contribution, we detail the record of propagating multi-segment and branching seismic ruptures and the related formation of dilational sites which are captured in these pseudotachylytes. In addition, we estimate source parameters for the seismicity recorded in these rocks.

Seismic slip in the Gairloch Shear Zone

Development of the Gairloch Shear Zone

The Gairloch Shear Zone (GSZ) in NW Scotland (Fig. 1a) consists of a series of Laxfordian high strain zones recording amphibolite to greenschist facies ductile deformation (Droop *et al*. 1999; Park 2010) and subsequent greenschist facies brittle deformation (Lei & Park 1993). The high strain zones are typically localised along lithological boundaries within the Loch Maree Group (LMG), a belt of Paleoproterozoic oceanic meta-basalts, meta-sedimentary rocks and meta-granodiorite (Fig. 1a)

83 interpreted as a 2.0-2.2 Ga island arc and accretionary complex from the Nagssugtoqidian–Lapland–
84 Kola collisional belt (Whitehouse *et al.* 1997; Park *et al.* 2001). The LMG is incorporated into the
85 Gairloch Terrane and 'southern region' of the Lewisian Complex (Kinny *et al.* 2005).

86 Lithologies affected by the high strain zones and brittle deformation include (Park *et al*. 2001): (a) a
87 layered suite of metasedimentary rocks, predominantly consisting of quartz-biotite semipelites with
88 minor contributions of calc-silicate-, quarzitic-, amphibolitic-, chloritic- and graphitic- schists; (b)
89 hornblende-plagioclase amphibolites, of which the larger bodies are meta-volcanics and the smaller
90 bodies metamorphosed Scourie Dykes; (c) Archean quartzo-feldspathic orthogneisses from the
91 basement of the LMG; (d) Paleoproterozoic quartzo-feldspathic orthogneiss, locally with variable
92 mafic composition. The amphibolites, which form the host rock to the faults discussed in this current
93 contribution, are typically dominated by hornblende with andesine-oligoclase plagioclase plus minor
94 and variable quartz, epidote, garnet, biotite and calcite (Park 1966).

95 Polyphase development of the viscous shear zones in the GSZ is thought to have occurred between
96 1800-1500 Ma (Moorbath & Park 1972, Lei & Park 1993; Park *et al.* 2001). The major phases of this
97 Laxfordian shear zone formation involved coeval amphibolite facies metamorphism, NW-SE
98 elongation, dextral and sinistral shear on complementary structures and a progressive steepening
99 and/or folding of structures (Lei & Park 1993). The subsequent late- and post-Laxfordian brittle
100 deformation was predominantly sinistral (Lei & Park 1993; Beacom *et al.* 2001), and included the
101 coseismic generation of pseudotachylytes (Park 1961; Sherlock *et al.* 2008). Late greenschist facies
102 retrogression is thought to have preceded the onset of brittle deformation (Lei & Park 1993).
103 Particularly intense bands of brittle fracturing and faulting were initially termed 'crush zones' (Peach
104 *et al.* 1907) and generally follow the NW-SE foliation of the shear zones, mapped as the Leth-
105 Chreige, Creag Bhan, Flowerdale, Tor an Easain, and Ialltaig - Mill na Claise belts (Lei & Park 1993).
106 Brittle faulting preceded the deposition of the Stoer Group sediments, and ^{40}Ar-^{39}Ar dating of the

pseudotachylytes in the Leth-Chreige crust belt date the seismicity there as 910 ± 19 to 1019 ± 19 Ma (Sherlock *et al.* 2008).

Pseudotachylytes within the brittle faults (Figs. 1b,c) were first identified by Park (1961), who confirmed their origin in frictional melting along brittle faults from observations of quench crystallization textures including spherulites and microlites. These observations pre-dated the understanding that pseudotachylytes were specifically generated by seismic slip (Sibson 1975; Cowan 1999; Rowe & Griffith 2015). Observations of pseudotachylytes within the GSZ have generally been confined to the crush belts along the boundaries between lithological units but also in isolated, heavily fractured regions within the gneisses and metapelites (Park 1961). Although the crush belts exploit boundaries with amphibolites, pseudotachylytes have so far only been described from within the gneisses and the metasedimentary rocks, with Park (1961) interpreting the amphibolites to have deformed via creep along the foliation. However, Beacom et al. (2001) characterise widespread foliation-parallel fracturing and cataclasites within the amphibolites, suggesting that frictional failure was accommodated within all lithologies.

Significance of pseudotachylytes in the Gairloch Shear Zone amphibolites

Contrary to previous studies of pseudotachylyte bearing faults in the Gairloch Shear Zone (Park 1961; Sherlock *et al.* 2008), we have focussed on the pseudotachylyte-bearing faults hosted in the foliated amphibolites of the Loch Maree Group. Amphibolite-hosted pseudotachylytes in the GSZ offer insights into the effects of pre-existing foliation on rupture geometry, as well as revealing the influence of an amphibole-dominated lithology. In contrast to many well studied pseudotachylyte-bearing exhumed fault zones hosted within felsic to intermediate plutonic rocks and weak-to-moderately foliated quartzo-feldspathic gneisses, for example the Gole Larghe Fault Zone (Di Toro *et al.* 2005a), Outer Hebrides Fault Zone (Sibson 1975), Mt. Abbot quadrangle, Sierra Nevada, (Griffith *et al.* 2008), Wenchuan Fault Zone (Wang *et al.* 2015), and the active Nojima Fault Zone (Otsuki *et al.* 2003), the amphibolite lithology and foliation-dominant microstructure make the study of the

seismic faults hosted within them novel. The amphibolite lithology hosting these GSZ pseudotachylytes is not common in reported pseudotachylyte-bearing exhumed fault zones, although amphibole-bearing metabasics are present in the pseudotachylyte-bearing Ivrea-Verbano Zone (Techmer *et al.* 1992) and Alpine Fault Zone (Toy *et al.* 2011). The GSZ therefore provides a rare opportunity to study the geological record of seismic faulting within a lithology which may be analogous to metamorphosed oceanic crust and subducting slabs (Rowe *et al.* 2005, Phillips et al. 2019). Additionally, because amphiboles melt under disequilibrium conditions at significantly lower temperatures than quartz and plagioclase (Spray 2010), we consider whether this influences the coseismic evolution of the slipping fault plane. Pseudotachylyte-fault zones hosted in anisotropic rocks of varying lithologies are not uncommon worldwide, and the geometry of GSZ pseudotachylyte faults show some similarity to those observed in mylonites in the Norumbega shear zone (Swanson 1988; Price *et al.* 2012) and the Ikertôq Shear Zone (Grocott 1981), and in foliated quartz-biotite gneisses in the Homestake Shear Zone (Allen 2005) in that the pseudotachylyte-bearing faults in the GSZ are often near-parallel to the foliation. However, initial observations of common pseudotachylyte fault geometries in the GSZ (Fig. 2) suggest that branching and linkage of fault planes typically create some discordance across the foliation. These processes are therefore significant in exploring how earthquake ruptures propagate in anisotropic rock.

Observations

In this study we look in detail at field and microstructural observations of pseudotachylyte faults from the GSZ to examine how examples of the different fault geometries initially identified in Fig. 2 may represent different processes influencing rupture complexity.

Host amphibolites and identification of pseudotachylytes

The sub-vertical NE-SE dipping amphibolite facies fabric is defined primarily by the shape preferred orientation of prismatic hornblende, whilst quartz and plagioclase tend to be more equant in shape. Hornblende is typically the most abundant phase, frequently comprising 50-75 % by area, and is also

157 the coarsest phase, with variable grain sizes between 50-1000 μm. In the samples studied here,
158 quartz and plagioclase are the next most abundant phases. Accessory phases include ilmenite,
159 apatite, rutile, and titanite, and retrogressive reaction products include epidote, chlorite, biotite and
160 calcite.

161 Pseudotachylytes hosted in amphibolites are reported here from several localities, all close (within
162 80 m) to lithological boundaries and/or reported crush zones (Fig, 1a). Within the amphibolites, the
163 pseudotachylytes share similar characteristics, typically displaying a pale yellow, grey or orange
164 weathering surface in the field (Fig. 1b), but on fresh surfaces unaltered samples are often pale grey
165 (Fig. 1c).

166 Pseudotachylytes are identified in thin section by the presence of melt-derived crystalline
167 microstructures, or by altered assemblages of these features (see Maddock 1983; Kirkpatrick and
168 Rowe 2013). The crystalline mineralogy of pseudotachylyte matrix – all phases that crystallized form
169 the melt - hosted within the GSZ amphibolites is predominantly composed of hornblende and
170 plagioclase with occasional augite. As reported by Park (1961), some GSZ pseudotachylytes have
171 completely recrystallized to fine-grained biotite and therefore have lost the morphological
172 characteristics of melt-derived crystallization. In thin section, the pseudotachylyte matrix is typically
173 dark brown and optically opaque (Figs. 3a,b). Many of the GSZ pseudotachylytes analysed in this
174 study preserve quench crystallization (or alternatively, devitrification from an initial quenched glass)
175 crystal morphologies such as dendritic amphibole and plagioclase, radiating crystals of plagioclase
176 and amphibole nucleating on unmelted survivor clasts (Figs. 3c) or forming spherical radiating
177 microlites (Figs. 3d). These microlites are formed of the largest crystals in the vein matrix, up to 50
178 μm in length, but the finer-grained crystalline fraction may be as fine as 2-3 μm. The finer-grained
179 phases are typically granular or lath-like (Figs. 3c,d). The grain size and morphology of the crystalline
180 matrix can vary with distance from the vein margin, creating a banded texture (Figs. 3b).

Unmelted survivor clasts occur throughout the veins and are usually rounded (Figs. 3a-c). Often these are monocrystalline and are dominated by quartz, plagioclase (oligoclase), and additionally apatite and titanite if these are present as accessory minerals in the host amphibolite. Polycrystalline clasts may also preserve hornblende and biotite (Figs. 3a). In selected examples, clasts of hornblende appear viscously deformed within a pseudotachylyte matrix that has no obvious solid-state viscous shear overprint (Figs. 3e), and ductile drag of hornblende is also seen locally adjacent to vein intersections (Figs. 3f). Within pseudotachylyte fault veins, the ratio of unmelted clasts to the crystalline melt-derived matrix has a mean value of 0.11 ± 0.08 (2 s.d.). Higher proportions of clasts seem to be associated with pseudotachylyte veins which are lighter brown in plane light, whereas low fractions occur in darker coloured matrices.

Macroscale geometry of pseudotachylyte veins

The simplest fault geometry observed in GSZ pseudotachylyte veins is a pseudotachylyte vein along an isolated planar fault which may display off-fault intrusions known as injection veins (Fig. 2a). These occur with a variety of aspect ratios and may curve (Fig. 1b), but they are defined by tensile fracture opening, in contrast to the shear fracture mode of the fault vein. Many GSZ pseudotachylyte faults, however, diverge from this basic configuration.

Segmented veins and overstepping

In places, pseudotachylyte fault veins parallel or sub-parallel to the amphibolite foliation form short sections which are linked by a step across foliation planes over separations of up to 2 cm centimetres (Figs. 2b,c, 4a). Not all of these pseudotachylyte fault veins are fully linked over the step, and instead are preserved as separate fault segments (Fig. 4b,c). In the example illustrated in Fig. 4, parallel fault vein segments overlap by ~ 1cm and show a pronounced curve at the tips inward towards the adjacent segment. Fig. 4c indicates narrow band of cataclased amphibolite has been partially overprinted by the central fault vein segment, which does not follow the band completely but instead curves up towards the adjacent fault vein segment. Micron-scale shear zones continue

beyond the curved vein tips, propagating onwards towards the adjacent vein in the form of a ductile fault-tip process zone (Fig. 4c-e). At other stepover sites within the same fault, the faults have linked and a through-going step in the vein is preserved (Fig. 4a,c). These linked steps often leave an abandoned segment tip, where only one fault segment completes the linkage across the step and the other is left as a straight overstep (Fig. 4c). The stepovers linked by a single tip are therefore typically narrower than the one in the upper half of Fig. 4c, where both segment tips have curved towards the adjacent segment. In a differing overstep-related geometry, rhombohedral pull-apart structures (Fig. 2c) have formed between overlapping pseudotachylyte fault segments, and may contain some centimetre-scale rounded clasts of the amphibolite (Fig. 5a).

Linkage of two parallel pseudotachylyte fault planes may be a systematic process along longer fault lengths, as in Fig. 2d. At the locality in Fig. 5b, pale pseudotachylyte occurs in planar veins in two dominant orientations, one parallel to the foliation and the other discordant. Both are restricted to an elongate tabular region around 10 cm wide with oblique foliation, bounded by planar discontinuities that locally also contain pseudotachylyte ('boundary faults', Fig. 5b). The oblique foliation and shear band structure in the amphibolite can be more clearly seen in the top left of Fig. 5c, in a locality where only a small volume of pseudotachylyte has formed. Internal veins within the shear band and discordant to the shear band foliation (Fig. 5b) appear to be minor faults with extensional sense of slip, based on the dilational accumulation of pseudotachylyte above the hanging wall of an internal fault. It is unclear if the internal foliation-parallel veins have any shear displacement across them. The discordant internal pseudotachylyte faults typically form an angle of ~ 55° from the boundary faults. In Fig. 5b, the pseudotachylyte is locally continuous across the two internal vein orientations and across into the boundary faults, but there is also a cross-cutting boundary between an extensional fault vein and a foliation parallel vein, suggesting that both sets of internal faults and the pseudotachylyte along them were created synchronously with slip along the boundary faults during an episode of seismic rupture. In Fig. 5b, a breccia is locally developed in the internal zone and rotation of the breccia clasts is apparent. Similarly, in the top right of Fig. 5c,

variable volumes of pseudotachylyte within the shear band create complex vein networks and brecciated domains. The lower shear band in Fig. 5c is here completely brecciated, with rounded, rotated clasts apparently supported by pseudotachylyte matrix.

Branching Faults

Branching faults (Fig. 2e) introduce discordant fault orientations and can be associated with complex pseudotachylyte vein networks (Figs. 5d-e). Branching faults in the GSZ often display intersections with an acute angle of 10-30° between the main fault and the secondary fault branch (Figs. 5d-f). The branch may split the main pseudotachylyte fault so that one fault vein has a thicker layer of pseudotachylyte than the other branch. The thicker branch may be either concordant or discordant to the foliation. At the branching tip of the fault in Figs. 5d, a network of small pseudotachylyte veins lie around the branching fault, forming a wider apparent damage zone than is usually observed around pseudotachylyte fault veins in the GSZ. In the fault branch in Fig. 5e, injection veins are developed in the intersection between the two branches, causing flame-like protrusions from the thicker fault branch. Closely-spaced fault branches may also be linked by brecciated domains (Fig. 5f).

Microscale geometry of pseudotachylyte veins

Vein margins

Whilst pseudotachylyte vein margins are generally planar, millimetre-scale stepping of the margins is common (Figs. 6a,b) which may be associated with sites of fracture and/or cataclasis in the wall-rock, or injection veins and smaller-scale roughness (Figs. 6a,b). This is distinct from later faulting which has also offset some of the pseudotachylyte veins, creating a similar stepped appearance. Preferential melting of the hornblende relative to plagioclase and quartz creates grain scale roughness and is observed at vein margins and also within polycrystalline clasts, where hornblende has melted but is surrounded by apparently intact quartz and plagioclase (Figs. 6c,d). Large

polycrystalline clasts may be removed from the margin by sidewall shortcut veins, which isolate blocks from the new vein margin and progressively smooth steps and curves out of the fault walls (Figs. 3a, 6e). These large clasts are initially little removed from their point of origin, but may be significantly rotated and exhibit internal faulting and injection of pseudotachylyte, resulting in progressive size reduction (Fig. 6e).

Injection veins

Small injection veins of pseudotachylyte away from the generation plane vary in geometry at the microscopic scale. Some stubby varieties appear to follow grain boundaries and may represent the exploitation of low melting point minerals, whilst others terminate with thin branches (Fig. 6f,g). Injections also propagate into clasts as well as into the margins and contribute to progressive fragmentation of the clasts (Fig. 6e). Some injection veins have rough margins, suggesting modification of the injection walls via melting.

Discussion

Seismic slip in the amphibolites of the Gairloch Shear Zone

The pseudotachylytes of the GSZ record frictional melting during seismic slip along faults in the amphibolites. Source parameters such as displacement, magnitude, and coseismic temperature, along with the depth of earthquake activity have not previously been attributed for these faults, so here we discuss what constraints may be placed on the nature of earthquake slip within the GSZ.

Relationship of seismic rupture with foliation and lithology

Within the GSZ, amphibolite-hosted pseudotachylyte-bearing faults are localised close to the lithological boundaries, but are not recorded along the actual boundary interfaces; indeed, they occur at distances up to 80 m laterally away from them. Exploitation of these boundary zones is also seen in pseudotachylyte faults occurring in the other lithologies that host the GSZ (Park 1961).

280 Spacing and orientation of fracturing has been observed to vary between the lithologies of the GSZ,
281 with amphibolites hosting typically foliation-parallel brittle deformation with a high factor of
282 clustering (Beacom *et al*. 2001). Such foliation-parallel fracture pattern is replicated in the
283 pseudotachylyte-bearing faults and is compatible with the understanding that strong anisotropy
284 tends to guide shear failure orientation, even if it is somewhat misorientated relative to the principal
285 stress directions (Donath 1961).

286 The amphibolite host rock presents a contrast in the thermal properties of its constituent minerals -
287 hornblende has a single-crystal melting temperature of 750 °C, whilst quartz and An_{30-50} plagioclase
288 will melt at ~1550° (if melting occurs before the high temperature phase change to β-christabolite)
289 and ~1350° respectively (Petzold & Hinz 1976; Spray 2010). Under disequilibrium frictional melting,
290 this leads to preferential melting of the amphibole, which is clearly illustrated by the clast in Figs. 6
291 c-d. In the wall of the fault, melting of amphibole between preserved quartz and plagioclase has led
292 to increased roughness of the fault surface on the grain scale (e.g. Fig. 6b), contrary to mechanical
293 wear processes that tend to smooth the fault walls with progressive slip (Brodsky *et al*. 2011),
294 examples of which may also be observed in these pseudotachylytes in the formation of sidewall
295 shortcuts (Figs. 3a, 6e). Preferential melting of amphibole is also observed in the walls of some
296 injection veins, indicating that the melt temperature in these off-fault tensile fractures also
297 remained above 750°C (Spray 2010) and hence was still molten at the tip of the vein, requiring
298 quenching to be slower than the fracture propagation (Rowe *et al.* 2012).

299 The volumetric ratio of survivor clasts relative to melt-derived matrix within any individual
300 pseudotachylyte fault vein is an indication of the thermodynamic balance between melting and
301 mechanical wear processes (O'Hara 2001). In the GSZ pseudotachylytes, the mean 2D clast to matrix
302 (representing the melt, includes microlites plus the finer-grained crystalline matrix) area ratio is 0.11,
303 at the lower boundary of the 0.1-0.7 range which has been previously reported for pseudotachylytes
304 from a collection of different fault zones (O'Hara 2001), indicating that an increased proportion of

melt was generated relative to products created purely by mechanical wear during slip. The breakdown of rock via mechanical wear and melting is influenced by the mineral yield strengths and thermal energy needed for melting, respectively. Although the ratio of these properties is fairly constant for many common minerals, amphiboles, particularly hornblende, have slightly lower melting points relative to their strength (O'Hara 2001; Spray 2010). Therefore, frictional melting of a hornblende-rich rock might be expected to generate an increased volume of melt along the fault relative to the volume of unmelted clasts, in comparison to a quartzo-feldspathic lithology. Additionally, even low coseismic temperature rises, associated with small increments of seismic slip, may still allow for widespread melting of the amphiboles. This relative ease of coseismic melt production may have implications for fault structure, with high melt pressures (i.e. fluid pressure) potentially contributing to opening tensile off-fault cracks (Swanson 1992) alongside dynamic rupture-tip stress fields (Di Toro *et al*. 2005b; Griffith *et al*. 2009; Ngo *et al*. 2012) and exploitation of pre-existing fractures. Interaction of locally high fluid pressure along the fault plane with the opening of dilational sites controlled by fault geometry will drive high fluid pressure gradients and consequential rapid flow of melt towards the dilational zone, potentially causing brecciation (Sibson 1975; Bjørnerud & Magloughlin 2004), all within the duration of coseismic slip. Hence, the interaction of the lithological control on melting and the foliation control on fault geometry has implications for the relative contributions of coseismic fault plane processes to the seismic energy budget and structural development of the fault zone.

Depth and temperature conditions of seismic faulting in the GSZ

The depth of brittle faulting and seismicity in the GSZ is not well constrained but occurred within lower greenschist facies temperatures (Park *et al*. 1987; Beacom *et al*. 2001) giving a likely ambient rock temperature between 250-350°. The geothermal gradient has been estimated for the GSZ as 22^{+7}_{-4} °C km^{-1} during Laxfordian ductile deformation phases (Droop *et al.* 1999). Whether this was still the case for the later brittle phase is not clear, but as Droop et al. (1999) regard this as a moderate

estimate for stable Precambrian crust, and considering the errors and the time-gap, we use an approximation of 25°C km^{-1} as the geothermal gradient in calculations. This gives a depth range of 9-13 km for the ambient temperature range 250-350°C.

Coseismic fault temperature, displacement, magnitude and slip direction

Pseudotachylyte-bearing faults in the GSZ capture individual episodes of seismic slip, thus capturing elements of the source parameters of the individual earthquakes. The energy budget required to melt a given volume of the host rock allows the coseismic heat rise in particular to be estimated, and is related to the seismic displacement, which scales with the seismic magnitude. Direct measurement of displacement in the field is not routinely possible in the GSZ, because there are few markers within the amphibolite that may be cut and offset across the faults. Calculating the necessary displacement required to produce a certain volume of pseudotachylyte melt is therefore a useful estimate on the magnitude of earthquake displacement recorded on these faults. The volume of coseismic melt is approximated by the average thickness of a pseudotachylyte fault vein (Di Toro *et al.* 2005a). Thickness measurements are best undertaken across fault veins with constant thickness and limited melt loss into sites such as injection veins and breccia. Although such geometrically simple veins are not common in the GSZ, a typical thickness of the pseudotachylyte along linear faults is around 5 mm (e.g. Fig. 4a). The relationship between the thickness of melt, the displacement and the thermal properties of the rock is

$$d = \frac{\rho . w}{\tau} \left[(1 - \phi) H + c_p (\Delta T) \right] \quad (1)$$

where d is the displacement, ρ the density, w the width of the vein, τ is the shear stress on the fault, ϕ is the area of clasts in the vein as a fraction of the total vein, H is latent heat of melting, c_p is the specific heat and ΔT is the difference between the coseismic melt temperature and the ambient temperature before and after the earthquake, T_{melt} - $T_{ambient}$ (Di Toro *et al*. 2005a). Values used for these parameters are given in Table 1. Values for the shear stress resolved along the fault are

354 estimated from the lithostatic stress state by equating the lithostatic stress (P_c = ρ.g.h, where g is
355 gravitational acceleration, and h is depth) with the mean stress of a strike-slip stress field. Assuming
356 a Poisson's ratio of 0.25 (Jaeger & Cook 1979) and an angle of 30° between the maximum principal
357 stress and the fault plane, this places the expected range of resolved shear stress at 107-155 MPa for
358 the estimated depth range of 9 to 13 km (Fig. 7a). Constraining ΔT relies on estimating the maximum
359 temperature reached by the coseismic melt (T_{melt}), which in many pseudotachylytes is reported
360 within the range ~1000-1500°C (O'Hara 2001; Di Toro & Pennacchioni 2004; Caggianelli *et al*. 2005;
361 Nestola *et al*. 2010) from a combination of thermal and thermodynamic modelling, matrix indicator
362 phases and melting temperatures of surviving clasts relative to melted phases. For the GSZ
363 pseudotachylytes we use the latter method, which places upper and lower bounds on the melt
364 temperature. The lower bound for the melt temperature is 750°C, the melting temperature of
365 hornblende. Plagioclase is partially preserved as unmelted survivor clasts, placing a reasonable
366 upper bound for coseismic fault plane temperature at the An_{30-50} melting temperature of 1350°C
367 (Spray 2010). Using these parameters in equation 1, the resulting mean values of coseismic
368 displacement equivalent to a pseudotachylyte thickness of 5 mm range from d = 123 ± 40 mm at 9
369 km depth to d = 76 ± 28 mm at 13 km depth (Fig. 7b), scaling inversely with depth-dependent shear
370 stress.

371 Earthquake magnitude for these events may be loosely constrained based on this displacement
372 range. The seismic moment, M_0, is related to the displacement (d), rupture area (A) and the shear
373 modulus (G) as M_0 = d.A.G. The typical rupture size on pseudotachylyte faults in the GSZ is
374 somewhat uncertain, because the pseudotachylyte extent may represent only part of a larger fault
375 plane that is not always fully exposed or easily traced (Kirkpatrick *et al.* 2012), especially if faults are
376 foliation parallel and/or segmented. Rupture area is calculated from fault length based on the
377 assumption of a circular fault with diameter equivalent to the fault length, a simplification of the
378 elliptical geometry solution demonstrated by Eshelby (1957). A reasonable range of GSZ fault lengths
379 (i.e. a maximum rupture length) would be between 1m and 100m, in which case the range of

moment magnitudes (M_w) converted from the seismic moment would be between 0.1 and 3.1 M_w based on the empirical relationship $M_W = \frac{Log\, M_0}{1.5} - 6.07$ (Kanamori & Brodsky 2004). The uncertainties arising from the unknown fault length are clearly large (Fig. 7b), but nonetheless illustrate that the many of the pseudotachylytes in the GSZ were generated by a series of relatively small magnitude earthquakes.

The slip direction of the brittle faults in the GSZ is typically thought to have been sinistral (Park *et al.* 1987; Beacom *et al.* 2001; Sherlock *et al*. 2008). The sense of slip on the pseudotachylyte faults presented here is frequently difficult to determine, but where evidence for slip direction exists there are also dextral examples (e.g. Fig. 5a), indicating that seismicity likely occurred with both apparent dextral and sinistral kinematics. This is not incompatible with a dominantly sinistral tectonic regime, because small ruptures that occur as aftershocks or which occur in the damage zone or even further away from the major fault planes are often observed to have varying slip senses in observations of present day seismicity (Cheng *et al.* 2018; Cooke & Beyer 2018).

Rupture geometry and dilational zones

Segmentation and branching

A common feature along GSZ pseudotachylyte-bearing faults is a stepover between parallel but laterally offset segments of the fault (e.g. Fig. 4, Fig. 5a, Fig. 8a-b). These macroscopically stepped faults represent linkage of several fault segments, which, in the examples seen, tend to lie parallel to the amphibolite foliation. There appears to be two mechanisms of linkage between fault segments containing pseudotachylytes in the GSZ. Firstly, there is linkage driven by curvature of the segment tips once they overlap with an adjacent segment (Fig. 8a). The best example of this process is illustrated in Fig. 4. This fault has a number of steps along strike, most of which have a completed through-going linkage linked and so evidence of the linkage mechanism is obscured. However, in the stepover detailed in Figs. 4b-e, linkage is not quite complete, and ductile shear zones are preserved ahead of the fault tips, representing the process zone that precedes a propagating shear fracture

(Misra *et al.* 2015). Both the overlapping tips display this process zone (Figs. 4d,e), indicating that both fault segments were propagating towards the other, in opposing directions (Fig. 8a). The presence of pseudotachylyte in the fault segments indicates that this propagation occurred during earthquake rupture, i.e. at least parts of these fault segments were newly formed during the earthquake which produced the pseudotachylyte, and the interaction of the segment tips indicates that all the segments must have been actively slipping during the same episode of coseismic rupture. Where linkage of the segments has occurred at other steps along the fault, the pseudotachylyte is continuous across the step, indicating that complete linkage of the segments also occurred during the same earthquake. A further implication is that nucleation of slip occurred at several sites on adjacent foliation planes, each growing into a short slip segment before a through-going slip plane was established. This fault therefore records the various stages of centimetre-scale growth, interaction and linkage of fault segments that can occur within a single earthquake, the duration of which is typically < 0.2 s for events < M_W 3 (Kanamori & Brodsky 2004). The growth of the through-going fault in this manner is very similar to the model of fault growth from segments which exploit pre-existing weaknesses (Segall & Pollard 1983), but in the case of the GSZ the initial weakness plane is probably the amphibolite foliation, although the apparent overprint of a cataclastic zone by the pseudotachylyte segment in Fig. 4c may indicate that pre-existing faults were partially exploited by the later rupture event recorded in the pseudotachylyte. The vein margins are frequently stepped at smaller scales of ~1 mm vein–normal separations (Figs. 6a,b) which suggests that segmentation of slip may be applicable at several scales, and that on rupture initiation slip may have nucleated simultaneously across a diffuse suite of foliation planes spaced only a few grains apart. Coalescence of these would have occurred forming the larger segments typically spaced ~1 cm apart (e.g. Fig. 4). After segment linkage or branching, the fault wall geometry would be liable to be progressively modified by processes such as the creation of sidewall-shortcuts (Figs. 3a, 6e) which act to smooth out steps in the vein by by-passing protruding asperities to create a more planar fault margin (Fig. 6e). This rip-out process has been linked specifically to strike-slip faulting along planes of anisotropy

(Swanson 1989) but in the GSZ appears to predominantly straighten curved or stepped faults rather than creating lensoid ramps into the fault walls from an initially planar fault, as in the model of Swanson (1989), likely due to the segmentation control on the initial fault geometry.

The curvature of overlapping segment tips (Fig. 4c) is an expression of the modification of the local fault tip stress field due to interaction between two closely-spaced overlapping cracks (Pollard *et al*. 1982; Pollard & Aydin 1984; Nicholson & Pollard 1985) which causes the propagation path to curve. This style of linkage is well-documented in dilatant crack systems including veins and dykes (Pollard *et al.* 1982; Nicholson & Pollard 1985), in contrast to shear planes which more typically form sets of secondary fractures and/or folds in the overstep region (Fig. 8b), rather than propagate the primary crack tips towards each other in this way. The pull-apart in Fig. 5a is an example of a typical extensional stepover between shear cracks (e.g. Sibson 1986) and is an example of the second mechanism of fault segment linkage demonstrated in the GSZ pseudotachylytes. In Fig. 5a, the fault is right-stepping and has an apparent dextral sense of slip, creating an extensional overstep which is now filled with a pseudotachylyte rhombocasm. These pull-apart stepovers are well documented between strike-slip fault segments and on releasing bends at all fault scales, from millimetre-width (Peacock & Sanderson 1995) to hundreds of kilometres (Mann *et al.* 1983), and are also well-described for pseudotachylyte-bearing faults (e.g. Sibson 1975). Unlike the crack-tip linkage (Fig. 8a), the multiple parallel slip segments do not necessarily need to exist pre-linkage because transfer of the rupture across to potential adjacent slip planes (the foliation, in the GSZ amphibolites) may occur via the formation of secondary faults in the future overstep (Sibson 1986; Harris *et al.* 1991; Melosh *et al.* 2014). Because this form of linkage is so common, it is interesting that the first mechanism via propagating crack tips also occurs across these faults, especially when it is more typical of dilatant mode I cracks (Pollard *et al.* 1982; Pollard & Aydin 1984). Some numerical models show that this curved propagation of crack tips can also occur on mode II shear fractures (Du & Aydin 1993; Ando *et al.* 2004). Alternatively, dilation of the fault segments could be introduced via local high fluid pressure driven by voluminous coseismic melt generation, leading the propagating

457 rupture to behave as hybrid extensional–shear fractures. High coseismic fluid pressure has several
458 implications for dynamic fault strength, potentially including transient loss of shear strength if the
459 fluid/melt pressure becomes equal to or greater than the normal stress on the fault. However,
460 evidence for high melt pressure is typically only locally seen in pseudotachylytes, for example in the
461 dynamic creation of pseudotachylyte injection veins at the fault tip (Rowe *et al.* 2012; Sawyer &
462 Resor 2017) and in breccias where extreme rotation of the clasts suggests fluid-supported implosion
463 (Bjørnerud & Magloughlin 2004). Along relatively simple fault geometries such as that shown in Fig.
464 4, where off-fault melt escape routes are not apparent, the melt has instead have been trapped
465 along the fault plane, forming a continuous film and influencing dilatant-crack geometries across the
466 propagating fault segments. Whichever the mechanism of segment linkage, the resultant stepped
467 fault geometry is also observed in kilometre scale active fault zones and in earthquake surface
468 rupture patterns (Tchalenko & Berberian 1975; Bilham & Williams 1985), indicating that some of the
469 processes of fault linkage observed in the GSZ pseudotachylytes could be potentially up-scaled.
470 However, the influence and interaction of coseismic melt-pressure and closely-spaced rupture tip
471 stress fields are perhaps not so easy to simply scale up across larger spatial distances.

472 Branching faults are common in the GSZ (Figs. 5d,e) and represent synchronous seismic slip on both
473 branches where the pseudotachylyte is continuous across the branch intersection (Rowe *et al*.
474 2018). Such branching is a recognised feature of kilometre-scale fault zones and can also be linked
475 on that scale to single earthquake ruptures (Poliakov *et al.* 2002; Fliss *et al.* 2005). Without good
476 evidence for sense of displacement across the GSZ faults it is difficult to interpret the kinematics of
477 these branches, as numerical models suggest that branching in both forward and backwards
478 directions relative to the direction of rupture propagation is possible (Fliss *et al.* 2005). As noted by
479 Rowe et al. (2018), intersecting branches that slip in the same rupture must also experience
480 different slip vectors and magnitudes of slip, so that the geometry has a direct influence on the
481 spatial heterogeneity of rupture source properties. In the observations of Rowe et al. (2018), two
482 thin fault branches coalesce into the wider main fault plane. We observe some additional detail by

noting that one fault branch is typically wider than the other (Figs. 5d,e), which may signify that relative differences in seismic slip speed or magnitude, and hence melt production, are common between coalescing branches. In the case of the branch in Fig. 5e, the discordant branch has a thicker pseudotachylyte vein and also appears to be longer than the other fault branch which forms an extension to the main fault vein and remains parallel to the foliation. Ruptures exploiting a pre-existing fault branch can sometimes terminate rupture on the main fault branch if the secondary branch has significant length and is inclined at a shallow angle to the main fault (Bhat et al., 2007), as in Fig 5e. Typically, this termination of rupture on the main fault occurs when the branch is situated in the extensional field of the propagating rupture tip (Bhat et al., 2007). This branch configuration might also encourage the development of tensile veining (Fig. 5e) and dilational brecciation (Fig. 5f) in the intersection of the fault branches, given accommodating slip on the secondary branch. In the cited models of branching faults (Fliss et al., 2005, Bhat et al., 2007) the secondary fault branches must exist as a pre-existing structure before the rupture in question is generated along the fault. Similarly, in cases such as Fig. 5e, where the secondary fault branch is discordant to the foliation, we suggest that some pre-existing heterogeneity within the amphibolite fabric may be necessary to divert the rupture down the secondary fault branch and away from the dominant plane of weakness formed by the foliation. In Fig. 5f, and also in Figs. 5b-c, branching faults within the confines of a paired fault zone are observed, in the sense that slip on the 'internal' faults is coeval and continuous with slip on the boundary faults, as indicated by brecciation in the branch intersection (Fig. 5f). However, in these cases the length of the secondary fault branch (the internal fault) is limited by the width of the controlling structure (the shear band), and so branching of the rupture along these small faults is unlikely to inhibit the continuing rupture along the main boundary fault, whatever the configuration of the secondary branch faults with respect to the main fault and stress field (Bhat et al., 2007).

Brecciation sites

Within the GSZ pseudotachylytes, there are several examples of localised dilation associated with coseismic slip and pseudotachylytes. These dilational sites are controlled by the fault geometry. Under the classification scheme of (Rowe *et al*. 2018), these can be described as angular breccias (Fig. 5f), pull-aparts/rhombocasms (Fig. 5a), and tabular breccias (Fig. 5c). The pseudotachylyte faults in the GSZ show progressive stages of breccia development, which illustrate how these features evolve (Fig. 8).

Angular breccias are associated with dilational sites within the intersections of branching faults (Fig. 5f), although they may potentially also form between oblique adjacent fault segments. In both cases, they signify coeval seismic slip on the bounding structures. Pull-aparts filled with pseudotachylyte may contain breccia clasts (Fig. 5a) and in the case of rhombochasms are typically formed by dilation at extensional stepovers between fault segments. These rhombohedral pull-aparts form via secondary tensile and shear fractures which form the through-going link between overlapping faults (Fig. 8b), and do not necessarily require fluid (including melt) to fragment the rock in the overlap (Sibson 1986; Melosh *et al*. 2014) although high fluid pressures may assist this process (Sibson 1975; Bjørnerud & Magloughlin 2004). A similar final geometry is formed via the crack-tip propagation mechanism of segment linkage, where the isolation of a 'bridge' between curving, overlapping fault tips and the resultant influx of melt might induce tensile fragmentation of the bridge (Fig. 8a) once it is surrounded by melt and confinement is lost (Nicholson & Pollard 1985). The resulting breccia geometry would be defined by the curvature of the fault segments, likely producing a more rectangular stepover breccia than the rhombohedral pull-aparts (Figs. 8a,b).

The tabular pseudotachylyte breccias in the GSZ portray clearly how these structures progressively form within a single earthquake (Fig. 8c). A pre-existing shear band has been reactivated by concurrent slip on both boundaries, with exploitation of the internal oblique foliation for pseudotachylyte injection and/or potential shearing (Fig. 5b). The geometry of this stage is very similar to the 'strike-slip duplexes' observed in the Ikertôq Shear Zone, Greenland (Grocott 1981)

533 and the Norumbega Shear Zone, US (Swanson 1988) where internal Riedel shear sets are a product
534 of interaction between the paired boundary faults and also may contain pseudotachylyte, as in the
535 GSZ examples. The offset on these internal faults implies that they are not a product of dynamic
536 tensile fracture as in the brecciation model of Melosh *et al.* (2014). In the GSZ the internal faults are
537 extensional and orientated at a moderately high angle to the boundary faults, suggesting that they
538 could be X-type Riedel shears which tend to indicate layer-parallel extension (Swanson 1988). This
539 condition is considered ideal for the progressive formation of breccias from paired fault zones
540 (Swanson 1988), which requires a combination of increasing internal fault formation combined with
541 increasing volumes of melt in the internal zone until catastrophic fragmentation brecciates domains
542 of the rock (Fig. 8c). In order for the paired fault zones to form, an anisotropic rock is thought to be
543 necessary, with Swanson (1988) suggesting that these may mainly form in mylonites near the base
544 of the seismogenic zone. However, the foliation in the Gairloch amphibolites, primarily defined by
545 parallel orientation of prismatic amphiboles, also provides an appropriate fabric, especially where
546 reinforced by pre-existing structural heterogeneities such as shear bands. Paired fault zones may
547 therefore be a feature, at least at this centimetre to metre scale, of any level in the brittle crust
548 where systematic anisotropy is present.

549 The presence of foliation also favours the progression to fragmentation and breccia formation due
550 to preferential utilisation of the foliation planes for fracturing (Melosh *et al*. 2014) and in the GSZ
551 this is supported by the injection of pseudotachylyte along the internal foliation planes (e.g. Fig. 5b).
552 It is not clear, however, whether this rupture geometry would be a feature of large tectonic scale
553 earthquakes. Riedel shears may form part of large ruptures (e.g. M_W 7.8 Kunlun earthquake, Lin and
554 Nishikawa 2011), and strike slip duplex geometries with paired boundary fault zones are observed at
555 5-10 km scales (Cembrano *et al.* 2005). However, the synchronous propagation of rupture both
556 along parallel segments (i.e. the paired boundary faults) has so far not been identified in active
557 earthquakes (Rowe *et al.* 2018). The mechanisms allowing the paired faults to propagate past each
558 other, rather than form linked stepovers similar to Fig. 8a, is therefore of interest, although once

559 the paired slip planes are in motion the process of forming the internal dilational pull-apart is
560 probably much the same (Sibson 1975; Cembrano *et al.* 2005). Such rupture geometries may
561 therefore be closely controlled by the spacing between the two faults (Harris *et al.* 1991; Ando *et al.*
562 2004) along with the favourability of the initial slip planes (Donath 1961). The aspect ratio of these
563 elongate structures is such that even if scaled up to tens of kilometres, the separation between the
564 boundary faults might be unresolvable at the spatial resolution of seismological observations or
565 from geodetic observations of surface deformation.

566 Context of seismicity recorded by pseudotachylytes in the GSZ

567 The GSZ records ~1 Ga seismicity hosted within foliated amphibolites and other lithologies. In the
568 amphibolites, the pseudotachylytes were formed by small magnitude (≤ M_W 3) earthquake ruptures
569 that frequently exploited the foliation within the host rock, but which have locally also branched,
570 stepped and brecciated volumes of the rock. These faults are scattered close to the lithological
571 boundaries which were thought to localise most of the brittle deformation (Lei & Park 1993), but no
572 pseudotachylytes in this study have been found to lie in the core of the crush belts along the actual
573 lithological interface itself, instead typically forming small fault clusters within ~100 m of the
574 boundary. It is expected that earthquakes would also rupture along the major heterogeneity of the
575 lithological boundaries, especially where the intensely fragmented 'crush zones' are observed (Fig.
576 1a), but repeated slip episodes combined with potential fault-focussed fluid influx and subsequent
577 alteration would likely fragment and overprint any pseudotachylyte produced there, making them
578 unrecognisable (Kirkpatrick & Rowe 2013). Many of these pseudotachylytes record a single episode
579 of slip, with only a couple of examples showing that an older pseudotachylyte has been cut through
580 by a later pseudotachylyte-bearing fault, or that a pseudotachylyte overprints cataclasite (e.g. Fig.
581 4c). This suggests that each new earthquake preferentially ruptured along a new fault plane, likely
582 because solidified pseudotachylytes tend to strengthen the fault planes they occur on within the
583 upper crust (Mitchell *et al.* 2016; Hayward & Cox 2017) if they avoid wholescale hydration and

584 alteration to phylosillicate-rich assemblages (Phillips et al., 2019). A possible model for these small
585 pseudotachylyte faults observed here would be scattered seismic slip occurring in the damage zone
586 of the principal slip plane along the lithological boundaries, much as has been suggested for
587 pseudotachylytes in exhumed sections of the Alpine Fault, New Zealand (Toy *et al.* 2011).

588 These pseudotachylytes record seismicity along brittle faults that occurred between 1019 and 910
589 Ma (Sherlock et al., 2008). Previous discussion of these dates found that there was not enough
590 resolution to distinguish whether the seismicity was a feature of late-Grenvillian or of post-
591 Grenvillian deformation (Sherlock et al., 2008). However, more recent recognition of the Valhalla
592 orogeny (1030-710 Ma) in the North Atlantic and, more specifically, its 980-910 Renlandian phase
593 (Cawood et al., 2010) provide a better fit to the pseudotachylyte ages of the GSZ. The metamorphic
594 signature of the Renlandian has recently been reported from Neoproterozoic Morar Group
595 metasedimentary rocks in NW Scotland (Bird et al., 2018), although prior to their Caledonian
596 transport in the hanging wall of the Moine Thrust (435-420 Ma, Streule et al., 2010) these
597 metasediments may have lain an additional ~80 km or more away from the GSZ (Elliot and Johnston,
598 1980). Meanwhile, Neoproterozoic Torridon group sediments unconformably deposited around
599 1080-980 Ma (Turnbull at el., 1996, Rainbird et al., 2001) onto the GSZ and the Loch Maree Group
600 (Fig. 1) are not metamorphosed. This would imply that, if the GSZ pseudotachylytes do represent
601 Renlandian deformation, that seismicity took place not much deeper than around 6 km, the
602 maximum known depositional thickness of the Torridon Group (Stewart, 2002) and the maximum
603 identified depth of burial of basal Torridon Group paleosols prior to the initiation of Caledonian
604 thrusting (Williams, 2015). This is shallower than the 9-13 km depth range for pseudotachylyte
605 generation estimated earlier in the discussion, although this estimation carried large uncertainty.
606 Another issue is that no pseudotachylytes or related faults are observed in the overlying Torridon
607 Group, requiring the basement and cover to have been completely uncoupled. This observation
608 previously led workers to infer that the pseudotachylytes pre-dated sediment deposition, but the
609 Applecross formation of the Torridon Group, also present in the GSZ area, is observed to have a low

elastic modulus (which would have been still lower prior to sediment consolidation) which could make it resistant to brittle failure (Ellis et al., 2012). Hence, they may not record obvious indicators of propagation of the seismic failure from the underlying GSZ, especially if, as is implied here, the seismicity was characterised by small-length scale, small magnitude earthquake ruptures. However, further uncertainty as to the relative timing and context of seismic, pseudotachylyte-generating faulting on the GSZ is presented by observations that the pseudotachylytes are cut by late normal faults (Sherlock et al., 2008) that are thought to be associated with extension related to the deposition of the Torridonian sediments (Beacom et al., 1999). More detailed field characterization of fault and fracture age relationships is needed in order to clarify this remaining uncertainty in timing and regional context of the seismicity.

Despite their age and small length scales, the pseudotachylytes in the amphibolites of the GSZ are well preserved and capture complex geometries and interactions of earthquake ruptures within anisotropic rock. It is important to recognise the controls on how these rupture geometries might have formed at all scales, because they display the conditions under which seismic rupture can propagate, or alternatively be arrested by, regions of geometrical complexity and separation along faults (Sibson 1985; Harris *et al*. 1991). Additionally, there has been increased recognition of complex ruptures with synchronous slip on multiple fault strands occurring in large recent earthquakes (e.g. Fletcher et al. 2016; Hamling et al. 2017; Ruppert et al. 2018). Understanding the controls on such ruptures can be enhanced by studying the geological record of seismicity in exhumed fault zones such as the GSZ.

Conclusions

The geometry of small-scale pseudotachylyte-bearing faults in the Gairloch Shear Zone record rupture geometries that are comparable with those of kilometre-scale large magnitude earthquakes. This geometry is influenced by the anisotropy of the foliation within the hosting amphibolites, and potentially also by the high coseismic fluid pressures that might result from voluminous frictional

melting of a lithology dominated by low melting point amphibole. A homogeneously distributed foliation led to multiple points of slip nucleation and a segmented fault structure during early rupture, followed by the interaction and linkage of adjacent segments as slip progressed. The interplay with high coseismic melt pressures may be evident in the dilational crack style of segment linkage and frequent occurrences of brecciated domains, creating a record of a variety of rupture geometries.

Acknowledgements

LC gratefully acknowledges funding from NERC (Studentship 1228272) and a National Museums Scotland CASE award which facilitated this work. We are grateful for constructive reviews from Eddie Dempsey and Joe Allen, which greatly improved the manuscript.

References

Allen, J.L. 2005. A multi-kilometer pseudotachylyte system as an exhumed record of earthquake rupture geometry at hypocentral depths (Colorado, USA). *Tectonophysics*, **402**, 37–54, https://doi.org/10.1016/j.tecto.2004.10.017.

Allen, J.L., O'Hara, K.D. & Moecher, D.P. 2002. Structural geometry and thermal history of pseudotachylyte from the Homestake shear zone, Sawatch Range, Colorado. *Field Guides* , **3**, 17–32, https://doi.org/10.1130/0-8137-0003-5.17.

Ando, R., Tada, T. & Yamashita, T. 2004. Dynamic evolution of a fault system through interactions between fault segments. *Journal of Geophysical Research: Solid Earth*, **109**, https://doi.org/10.1029/2003JB002665.

Beacom, L.E., Anderson, T.B. & Holdsworth, R.E. 1999. Using basement-hosted clastic dykes as syn-rifting palaeostress indicators: an example from the basal Stoer Group, northwest Scotland. *Geological Magazine*, **136**, S0016756899002605, https://doi.org/10.1017/S0016756899002605.

Beacom, L.E., Holdsworth, R.E., McCaffrey, K.J.W. & Anderson, T.B. 2001. A quantitative study of the influence of pre-existing compositional and fabric heterogeneities upon fracture-zone development during basement reactivation. *In*: Holdsworth, R. E., Strachan, R. A., Magloughlin, J. F. & Knipe, R. J. (eds) *Nature and Tectonic Significance of Fault Zone Weakening*. Bath, Geological Soc Publishing House, 195–211., https://doi.org/10.1144/gsl.sp.2001.186.01.12.

Bhat, H.S., Olives, M., Dmowska, R. & Rice, J.R. 2007. Role of fault branches in earthquake rupture dynamics. *Journal of Geophysical Research: Solid Earth*, **112**, https://doi.org/10.1029/2007JB005027.

Bilham, R. & Williams, P. 1985. Sawtooth segmentation and deformation processes on the southern San Andreas Fault, California. *Geophysical Research Letters*, **12**, 557–560, https://doi.org/10.1029/GL012i009p00557.

Bird, A., Cutts, K., Strachan, R., Thirlwall, M. F., & Hand, M. (2018). First evidence of Renlandian (c. 950–940 Ma) orogeny in mainland Scotland: Implications for the status of the Moine Supergroup and circum-North Atlantic correlations. *Precambrian Research*, ***305***, 283–294. https://doi.org/https://doi.org/10.1016/j.precamres.2017.12.019

Bjørnerud, M. & Magloughlin, J.F. 2004. Pressure-related feedback processes in the generation of pseudotachylytes. *Journal of Structural Geology*, **26**, 2317–2323, https://doi.org/http://dx.doi.org/10.1016/j.jsg.2002.08.001.

Brodsky, E.E., Gilchrist, J.J., Sagy, A. & Collettini, C. 2011. Faults smooth gradually as a function of slip. *Earth and Planetary Science Letters*, **302**, 185–193, https://doi.org/10.1016/j.epsl.2010.12.010.

Caggianelli, A., de Lorenzo, S. & Prosser, G. 2005. Modelling the heat pulses generated on a fault plane during coseismic slip: Inferences from the pseudotachylites of the Copanello cliffs

(Calabria, Italy). *Tectonophysics*, **405**, 99–119, https://doi.org/http://dx.doi.org/10.1016/j.tecto.2005.05.017.

Cembrano, J., González, G., Arancibia, G., Ahumada, I., Olivares, V. & Herrera, V. 2005. Fault zone development and strain partitioning in an extensional strike-slip duplex: A case study from the Mesozoic Atacama fault system, Northern Chile. *Tectonophysics*, **400**, 105–125, https://doi.org/https://doi.org/10.1016/j.tecto.2005.02.012.

Cheng, Y., Ross, Z.E. & Ben-Zion, Y. 2018. Diverse Volumetric Faulting Patterns in the San Jacinto Fault Zone. *Journal of Geophysical Research: Solid Earth*, **123**, 5068–5081, https://doi.org/10.1029/2017JB015408.

Cooke, M.L. & Beyer, J.L. 2018. Off-Fault Focal Mechanisms Not Representative of Interseismic Fault Loading Suggest Deep Creep on the Northern San Jacinto Fault. *Geophysical Research Letters*, **45**, 8976–8984, https://doi.org/10.1029/2018GL078932.

Cowan, D.S. 1999. Do faults preserve a record of seismic slip? A field geologist's opinion. *Journal of Structural Geology*, **21**, 995–1001, https://doi.org/10.1016/S0191-8141(99)00046-2.

Di Toro, G. & Pennacchioni, G. 2004. Superheated friction-induced melts in zoned pseudotachylytes within the Adamello tonalites (Italian Southern Alps). *Journal of Structural Geology*, **26**, 1783–1801, https://doi.org/10.1016/j.jsg.2004.03.001.

Di Toro, G. & Pennacchioni, G. 2005. Fault plane processes and mesoscopic structure of a strong-type seismogenic fault in tonalites (Adamello batholith, Southern Alps). *Tectonophysics*, **402**, 55–80, https://doi.org/http://dx.doi.org/10.1016/j.tecto.2004.12.036.

Di Toro, G., Pennacchioni, G. & Teza, G. 2005a. Can pseudotachylytes be used to infer earthquake source parameters? An example of limitations in the study of exhumed faults. *Tectonophysics*, **402**, 3–20, https://doi.org/10.1016/j.tecto.2004.10.014.

Di Toro, G., Nielsen, S. & Pennacchioni, G. 2005b. Earthquake rupture dynamics frozen in exhumed ancient faults. *Nature*, **436**, 1009–1012, https://doi.org/http://www.nature.com/nature/journal/v436/n7053/suppinfo/nature03910_S1.html.

Donath, F.A. 1961. Experimental study of shear failure in anisotropic rocks. *Geological Society of America Bulletin*, **72**, 985–989, https://doi.org/10.1130/0016-7606(1961)72[985:ESOSFI]2.0.CO;2.

Droop, G.T.R., Fernandes, L.A.D. & Shaw, S. 1999. Laxfordian metamorphic conditions of the Palaeoproterozoic Loch Maree Group, Lewisian Complex, NW Scotland. *Scottish Journal of Geology*, **35**, 31–50, https://doi.org/10.1144/sjg35010031.

Du, Y. & Aydin, A. 1993. The maximum distortional strain energy density criterion for shear fracture propagation With applications to the growth paths of En Échelon faults. *Geophysical Research Letters*, **20**, 1091–1094, https://doi.org/10.1029/93GL01238.

Elliott, D., & Johnson, M. R. W. (1980). Structural evolution in the northern part of the Moine thrust belt, NW Scotland. *Transactions of the Royal Society of Edinburgh: Earth Sciences*, *71*(2), 69–96. https://doi.org/DOI: 10.1017/S0263593300013523

Ellis, M. A., Laubach, S. E., Eichhubl, P., Olson, J. E., & Hargrove, P. (2012). Fracture development and diagenesis of Torridon Group Applecross Formation, near An Teallach, NW Scotland: millennia of brittle deformation resilience? *Journal of the Geological Society*, *169*(3), 297 LP – 310. https://doi.org/10.1144/0016-76492011-086

726 Eshelby, J. D. (1957). The determination of the elastic field of an ellipsoidal inclusion, and related
727 problems. *Proceedings of the Royal Society of London A: Mathematical, Physical and*
728 *Engineering Sciences* **241**, 376–396.

729 Ferrand, T.P., Labrousse, L., Eloy, G., Fabbri, O., Hilairet, N. & Schubnel, A. 2018. Energy Balance
730 From a Mantle Pseudotachylyte, Balmuccia, Italy. *Journal of Geophysical Research: Solid Earth*,
731 **123**, 3943–3967, https://doi.org/10.1002/2017JB014795.

732 Fletcher, J.M., Oskin, M.E. & Teran, O.J. 2016. The role of a keystone fault in triggering the complex
733 El Mayor–Cucapah earthquake rupture. *Nature Geoscience*, **9**, 303.

734 Fliss, S., Bhat, H.S., Dmowska, R. & Rice, J.R. 2005. Fault branching and rupture directivity. *Journal of*
735 *Geophysical Research: Solid Earth*, **110**, https://doi.org/10.1029/2004JB003368.

736 Griffith, W.A. & Prakash, V. 2015. Integrating field observations and fracture mechanics models to
737 constrain seismic source parameters for ancient earthquakes. *Geology* , **43**, 763–766,
738 https://doi.org/10.1130/G36773.1.

739 Griffith, W.A., Di Toro, G., Pennacchioni, G. & Pollard, D.D. 2008. Thin pseudotachylytes in faults of
740 the Mt. Abbot quadrangle, Sierra Nevada: Physical constraints for small seismic slip events.
741 *Journal of Structural Geology*, **30**, 1086–1094,
742 https://doi.org/http://dx.doi.org/10.1016/j.jsg.2008.05.003.

743 Griffith, W.A., Rosakis, A., Pollard, D.D. & Ko, C.W. 2009. Dynamic rupture experiments elucidate
744 tensile crack development during propagating earthquake ruptures. *Geology* , **37**, 795–798,
745 https://doi.org/10.1130/G30064A.1.

746 Griffith, W.A., Nielsen, S., Di Toro, G. & Smith, S.A.F. 2010. Rough faults, distributed weakening, and
747 off-fault deformation. *Journal of Geophysical Research: Solid Earth*, **115**, B08409,
748 https://doi.org/10.1029/2009jb006925.

749 Grocott, J. 1981. Fracture geometry of pseudotachylyte generation zones: a study of shear fractures
750 formed during seismic events. *Journal of Structural Geology*, **3**, 169–178,
751 https://doi.org/10.1016/0191-8141(81)90012-2.

752 Hacker, B.R., Abers, G.A. & Peacock, S.M. 2003. Subduction factory 1. Theoretical mineralogy,
753 densities, seismic wave speeds, and H2O contents. *Journal of Geophysical Research: Solid*
754 *Earth*, **108**, https://doi.org/10.1029/2001JB001127.

755 Hamling, I.J., Hreinsdóttir, S., et al. 2017. Complex multifault rupture during the 2016
756 M_w 7.8 Kaikōura earthquake, New Zealand.
757 *Science*, **356**.

758 Harris, R.A., Archuleta, R.J. & Day, S.M. 1991. Fault steps and the dynamic rupture process: 2-D
759 numerical simulations of a spontaneously propagating shear fracture. *Geophysical Research*
760 *Letters*, **18**, 893–896, https://doi.org/10.1029/91GL01061.

761 Hayward, K.S. & Cox, S.F. 2017. Melt Welding and Its Role in Fault Reactivation and Localization of
762 Fracture Damage in Seismically Active Faults. *Journal of Geophysical Research: Solid Earth*, **122**,
763 9689–9713, https://doi.org/10.1002/2017JB014903.

764 Holland, T.J.B. & Powell, R. 2004. An internally consistent thermodynamic data set for phases of
765 petrological interest. *Journal of Metamorphic Geology*, **16**, 309–343,
766 https://doi.org/10.1111/j.1525-1314.1998.00140.x.

767 Jaeger, J.C. & Cook, N.G.W. 1979. *Fundamentals of Rock Mechanics*, 3rd ed. London, Chapman &
768 Hall.

769 Kanamori, H. & Brodsky, E. 2004. The physics of earthquakes. *Reports on Progress in Physics*, **67**,
770 1429.

771 Kinny, P.D., Friend, C.R.L. & Love, G.J. 2005. Proposal for a terrane-based nomenclature for the
772 Lewisian Gneiss Complex of NW Scotland. *Journal of the Geological Society*, **162**, 175–186,
773 https://doi.org/10.1144/0016-764903-149.

774 Kirkpatrick, J.D. & Rowe, C.D. 2013. Disappearing ink: How pseudotachylytes are lost from the rock
775 record. *Journal of Structural Geology*, **52**, 183–198,
776 https://doi.org/http://dx.doi.org/10.1016/j.jsg.2013.03.003.

777 Kirkpatrick, J.D. & Shipton, Z.K. 2009. Geologic evidence for multiple slip weakening mechanisms
778 during seismic slip in crystalline rock. *J. Geophys. Res.*, **114**, B12401,
779 https://doi.org/10.1029/2008jb006037.

780 Kirkpatrick, J.D., Dobson, K.J., Mark, D.F., Shipton, Z.K., Brodsky, E.E. & Stuart, F.M. 2012. The depth
781 of pseudotachylyte formation from detailed thermochronology and constraints on coseismic
782 stress drop variability. *J. Geophys. Res.*, **117**, B06406, https://doi.org/10.1029/2011jb008846.

783 Lei, S. & Park, R.G. 1993. Reversals of movement sense in Lewisian brittle-ductile shear zones at
784 Gairloch, NW Scotland, in the context of Laxfordian kinematic history. *Scottish Journal of*
785 *Geology*, **29**, 9–19, https://doi.org/10.1144/sjg29010009.

786 Lin, A. & Nishikawa, M. 2011. Riedel shear structures in the co-seismic surface rupture zone
787 produced by the 2001 Mw 7.8 Kunlun earthquake, northern Tibetan Plateau. *Journal of*
788 *Structural Geology*, **33**, 1302–1311,
789 https://doi.org/http://dx.doi.org/10.1016/j.jsg.2011.07.003.

790 Maddock, R.H. 1983. Melt origin of fault-generated pseudotachylytes demonstrated by textures.
791 *Geology*, **11**, 105–108, https://doi.org/10.1130/0091-7613(1983)11<105:moofpd>2.0.co;2.

792 Mann, P., Hempton, M.R., Bradley, D.C. & Burke, K. 1983. Development of Pull-Apart Basins. *The*
793 *Journal of Geology*, **91**, 529–554, https://doi.org/10.1086/628803.

794 Melosh, B.L., Rowe, C.D., Smit, L., Groenewald, C., Lambert, C.W. & Macey, P. 2014. Snap, Crackle,
795 Pop: Dilational fault breccias record seismic slip below the brittle–plastic transition. *Earth and*
796 *Planetary Science Letters*, **403**, 432–445,
797 https://doi.org/http://dx.doi.org/10.1016/j.epsl.2014.07.002.

798 Misra, S., Ellis, S. & Mandal, N. 2015. Fault damage zones in mechanically layered rocks: The effects
799 of planar anisotropy. *Journal of Geophysical Research: Solid Earth*, **120**, 5432–5452,
800 https://doi.org/10.1002/2014JB011780.

801 Mitchell, T.M., Toy, V., Di Toro, G., Renner, J. & Sibson, R.H. 2016. Fault welding by pseudotachylyte
802 formation. *Geology* , https://doi.org/10.1130/G38373.1.

803 Moorbath, S. & Park, R.G. 1972. The Lewisian chronology of the southern region of the Scottish
804 mainland. *Scottish Journal of Geology*, **8**, 51 LP – 74, https://doi.org/10.1144/sjg08010051.

805 Nestola, F., Mittempergher, S., Toro, G.D., Zorzi, F. & Pedron, D. 2010. Evidence of dmisteinbergite
806 (hexagonal form of CaAl2Si 2O8) in pseudotachylyte: A tool to constrain the thermal history of
807 a seismic event. *American Mineralogist*, **95**, 405–409.

808 Ngo, D., Huang, Y., Rosakis, A., Griffith, W.A. & Pollard, D. 2012. Off-fault tensile cracks: A link
809 between geological fault observations, lab experiments, and dynamic rupture models. *Journal*
810 *of Geophysical Research: Solid Earth*, **117**, B01307, https://doi.org/10.1029/2011jb008577.

Nicholson, R. & Pollard, D.D. 1985. Dilation and linkage of echelon cracks. *Journal of Structural Geology*, **7**, 583–590, https://doi.org/https://doi.org/10.1016/0191-8141(85)90030-6.

Nissen, E., Elliott, J.R., et al. 2016. Limitations of rupture forecasting exposed by instantaneously triggered earthquake doublet. *Nature Geosci*, **9**, 330–336.

O'Hara, K.D. 2001. A pseudotachylyte geothermometer. *Journal of Structural Geology*, **23**, 1345–1357.

Ohno, I. 1995. Temperature Variation of Elastic Properties of α-Quartz up to the α-β Transition. *Journal of Physics of the Earth*, **43**, 157–169, https://doi.org/10.4294/jpe1952.43.157.

Otsuki, K., Monzawa, N. & Nagase, T. 2003. Fluidization and melting of fault gouge during seismic slip: Identification in the Nojima fault zone and implications for focal earthquake mechanisms. *Journal of Geophysical Research: Solid Earth*, **108**, 2192, https://doi.org/10.1029/2001jb001711.

Park, R.G. 1961. The pseudotachylite of the Gairloch District, Ross-shire, Scotland. *American Journal of Science*, **259**, 542–550, https://doi.org/10.2475/ajs.259.7.542.

Park, R.G. 1966. Nature and origin of Lewisian basic rocks of Gairloch, Ross-shire. *Scottish Journal of Geology*, **2**, 179 LP-199.

Park, R.G. 2010. Structure and evolution of the Lewisian Gairloch shear zone: variable movement directions in a strike-slip regime. *Scottish Journal of Geology*, **46**, 31–44, https://doi.org/10.1144/0036-9276/01-405.

Park, R.G., Crane, A. & Niamatullah, M. 1987. Early Proterozoic structure and kinematic evolution of the southern mainland Lewisian. *Geological Society, London, Special Publications*, **27**, 139–151, https://doi.org/10.1144/gsl.sp.1987.027.01.12.

Park, R.G., Tarney, J. & Connelly, J.N. 2001. The Loch Maree Group: Palaeoproterozoic subduction-accretion complex in the Lewisian of NW Scotland. *Precambrian Research*, **105**, 205–226, https://doi.org/10.1016/s0301-9268(00)00112-1.

Peach, B.N., Horne, J., Gunn, W., Clough, C.T. & Teall, J.J.H. 1907. *The Geological Structure of the North-West Highlands of Scotland*. Glasgow, HM Stationary Office.

Peacock, D.C.P. & Sanderson, D.J. 1995. Pull-aparts, shear fractures and pressure solution. *Tectonophysics*, **241**, 1–13, https://doi.org/https://doi.org/10.1016/0040-1951(94)00184-B.

Petzold, A. & Hinz, W. 1976. *Silikatchemie*. Leipzig, VEB.

Poliakov, A.N.B., Dmowska, R. & Rice, J.R. 2002. Dynamic shear rupture interactions with fault bends and off-axis secondary faulting. *Journal of Geophysical Research: Solid Earth*, **107**, 2295, https://doi.org/10.1029/2001JB000572.

Pollard, D.D. & Aydin, A. 1984. Propagation and linkage of oceanic ridge segments. *Journal of Geophysical Research: Solid Earth*, **89**, 10017–10028, https://doi.org/10.1029/JB089iB12p10017.

Pollard, D.D., Segall, P. & Delaney, P.T. 1982. Formation and interpretation of dilatant echelon cracks. *Geological Society of America Bulletin*, **93**, 1291–1303, https://doi.org/10.1130/0016-7606(1982)93<1291:FAIODE>2.0.CO;2.

Price, N.A., Johnson, S.E., Gerbi, C.C. & West, D.P. 2012. Identifying deformed pseudotachylyte and its influence on the strength and evolution of a crustal shear zone at the base of the seismogenic zone. *Tectonophysics*, **518–521**, 63–83,

https://doi.org/10.1016/j.tecto.2011.11.011.

Rainbird, R. H., Hamilton, M. A., & Young, G. M. (2001). Detrital zircon geochronology and provenance of the Torridonian, NW Scotland. *Journal of the Geological Society*, *158*(1), 15–27. https://doi.org/10.1144/jgs.158.1.15

Robie, R.A., Hemingway, B.S. & Fisher, J.R. 1979. *Thermodynamic Properties of Minerals and Related Substances at 298.15 K and 1 Bar (105 Pascals) Pressure and at Higher Temperatures*. Washington.

Rowe, C.D. & Griffith, W.A. 2015. Do faults preserve a record of seismic slip: A second opinion. *Journal of Structural Geology*, **78**, 1–26, https://doi.org/http://dx.doi.org/10.1016/j.jsg.2015.06.006.

Rowe, C.D., Moore, J.C., Meneghini, F. & McKeirnan, A.W. 2005. Large-scale pseudotachylytes and fluidized cataclasites from an ancient subduction thrust fault. *Geology*, **33**, 937–940, https://doi.org/10.1130/g21856.1.

Rowe, C.D., Meneghini, F. & Moore, J.C. 2011. Textural record of the seismic cycle: strain-rate variation in an ancient subduction thrust. *Geological Society, London, Special Publications*, **359**, 77–95, https://doi.org/10.1144/sp359.5.

Rowe, C.D., Kirkpatrick, J.D. & Brodsky, E.E. 2012. Fault rock injections record paleo-earthquakes. *Earth and Planetary Science Letters*, **335**–**336**, 154–166, https://doi.org/10.1016/j.epsl.2012.04.015.

Rowe, C.D., Ross, C., et al. 2018. Geometric Complexity of Earthquake Rupture Surfaces Preserved in Pseudotachylyte Networks. *Journal of Geophysical Research: Solid Earth*, **123**, 7998–8015, https://doi.org/10.1029/2018JB016192.

Ruppert, N.A., Rollins, C., Zhang, A., Meng, L., Holtkamp, S.G., West, M.E. & Freymueller, J.T. 2018. Complex Faulting and Triggered Rupture During the 2018 MW 7.9 Offshore Kodiak, Alaska, Earthquake. *Geophysical Research Letters*, **45**, 7533–7541, https://doi.org/10.1029/2018GL078931.

Sawyer, W.J. & Resor, P.G. 2017. Modeling frictional melt injection to constrain coseismic physical conditions. *Earth and Planetary Science Letters*, **469**, 53–63, https://doi.org/https://doi.org/10.1016/j.epsl.2017.04.012.

Segall, P. & Pollard, D.D. 1983. Nucleation and growth of strike slip faults in granite. *Journal of Geophysical Research: Solid Earth*, **88**, 555–568, https://doi.org/10.1029/JB088iB01p00555.

Sherlock, S.C., Jones, K.A. & Park, R.G. 2008. Grenville-age pseudotachylite in the Lewisian: laserprobe 40Ar/39Ar ages from the Gairloch region of Scotland (UK). *Journal of the Geological Society*, **165**, 73–83, https://doi.org/10.1144/0016-76492006-134.

Sibson, R. 1986. Brecciation processes in fault zones: Inferences from earthquake rupturing. *Pure and Applied Geophysics*, **124**, 159–175, https://doi.org/10.1007/bf00875724.

Sibson, R.H. 1975. Generation of peseudotachylyte by ancient seismic faulting. *Geophysical Journal of the Royal Astronomical Society*, **43**, 775, https://doi.org/10.1111/j.1365-246X.1975.tb06195.x.

Sibson, R.H. 1985. Stopping of earthquake ruptures at dilational fault jogs. *Nature*, **316**, 248.

Spray, J.G. 2010. Frictional Melting Processes in Planetary Materials: From Hypervelocity Impact to Earthquakes Jeanloz, R. & Freeman, K. H. (eds). *Annual Review of Earth and Planetary Sciences*,

38, 221–254, https://doi.org/10.1146/annurev.earth.031208.100045.

Stewart, A. D. (2002). *The later Proterozoic Torridonian rocks of Scotland; their sedimentology, geochemistry and origin*. Bath: Geological Society of London.

Streule, M. J., Strachan, R. A., Searle, M. P., & Law, R. D. (2010). Comparing Tibet-Himalayan and Caledonian crustal architecture, evolution and mountain building processes. *Geological Society, London, Special Publications*, *335*(1), 207–232. https://doi.org/10.1144/sp335.10

Swanson, M.T. 1988. Pseudotachylyte-bearing strike-slip duplex structures in the Fort Foster Brittle Zone, S. Maine. *Journal of Structural Geology*, **10**, 813–828, https://doi.org/http://dx.doi.org/10.1016/0191-8141(88)90097-1.

Swanson, M.T. 1989. Sidewall ripouts in strike-slip faults. *Journal of Structural Geology*, **11**, 933–948, https://doi.org/https://doi.org/10.1016/0191-8141(89)90045-X.

Swanson, M.T. 1992. Fault structure, wear mechanisms and rupture processes in pseudotachylyte generation. *Tectonophysics*, **204**, 223–242, https://doi.org/10.1016/0040-1951(92)90309-T.

Swanson, M.T. 2005. Geometry and kinematics of adhesive wear in brittle strike-slip fault zones. *Journal of Structural Geology*, **27**, 871–887, https://doi.org/10.1016/j.jsg.2004.11.009.

Tchalenko, J.S. & Berberian, M. 1975. Dasht-e Bayaz Fault, Iran: Earthquake and Earlier Related Structures in Bed Rock. *GSA Bulletin*, **86**, 703–709.

Techmer, K.S., Ahrendt, H. & Weber, K. 1992. The development of pseudotachylyte in the Ivrea—Verbano Zone of the Italian Alps. *Tectonophysics*, **204**, 307–322, https://doi.org/https://doi.org/10.1016/0040-1951(92)90314-V.

Toy, V.G., Ritchie, S. & Sibson, R.H. 2011. Diverse habitats of pseudotachylytes in the Alpine Fault Zone and relationships to current seismicity Fagereng, A., Toy, V. G. & Rowland, J. V (eds). *Geological Society, London, Special Publications*, **359**, 115–133, https://doi.org/10.1144/sp359.7.

Turnbull, M. J. M., Whitehouse, M. J., & Moorbath, S. (1996). New isotopic age determinations for the Torridonian, NW Scotland. *Journal of the Geological Society*, *153*(6), 955–964.

Ujiie, K., Yamaguchi, H., Sakaguchi, A. & Toh, S. 2007. Pseudotachylytes in an ancient accretionary complex and implications for melt lubrication during subduction zone earthquakes. *Journal of Structural Geology*, **29**, 599–613, https://doi.org/http://dx.doi.org/10.1016/j.jsg.2006.10.012.

Wang, H., Li, H., Janssen, C., Sun, Z. & Si, J. 2015. Multiple generations of pseudotachylyte in the Wenchuan fault zone and their implications for coseismic weakening. *Journal of Structural Geology*, **74**, 159–171, https://doi.org/http://dx.doi.org/10.1016/j.jsg.2015.03.007.

Whitehouse, M.J., Bridgwater, D. & Park, R.G. 1997. Detrital zircon ages from the Loch Maree Group, Lewisian Complex, NW Scotland: confirmation of a Palaeoproterozoic Laurentia—Fennoscandia connection. *Terra Nova*, **9**, 260–263, https://doi.org/10.1111/j.1365-3121.1997.tb00025.x.

Tables

Parameter	Description	Value	Source
ρ	density	2809 kg m^{-3}	[a]
w	pseudotachylyte width	0.005 m	
τ	shear stress on fault	107-155 MPa	See Fig. 7a
ϕ	ratio of clasts to crystalline matrix	0.11	
H	latent heat of melting	135213 J kg^{-1}	[a]
c_P	specific heat	1017 J kg^{-1} K^{-1}	[a]
T_{melt}	coseismic melt temperature	1023 - 1623 K	[b]
$T_{ambient}$	ambient host rock temperature	518-618 K	[c]
G	shear modulus	49 GPa	[d]

Table 1: *Thermal and mechanical properties attributed to the GSZ amphibolite and the pseudotachylyte faults within them. Obtained from [a] values for tremolite, anorthite and quartz in Robie et al. (1979); [b] melting temperatures for hornblende and oligoclase in Spray (2010); [c] geothermal gradient of 25°C km^{-1}, modified from Droop et al. (1999); [d] values for hornblende, anorthite and quartz presented in Hacker et al. (2003) and originally sourced from Ohno (1995) and Holland & Powell (2004).*

Figure captions

Figure 1. Pseudotachylyte in the Gairloch Shear Zone: **(a)** Location of the Gairloch Shear Zone and simplified lithological map (modified from Lei & Park 1993) showing localities where pseudotachylytes are found within amphibolites; **(b)** typical yellow-grey weathered pseudotachylyte within foliated amphibolite - the pseudotachylyte veins here includes the generating fault vein (indicated by white arrowheads) plus injection veins protruding at a high angle from the fault [57.7122°N 05.6240°W]; **(c)** typical grey fresh surface of pseudotachylyte, two overlapping pseudotachylyte veins within darker amphibolite [57.7066°N 05.6173°W].

Figure 2. Idealised types of pseudotachylyte (PST) fault vein geometries observed in the Gairloch Shear Zone amphibolites: **(a)** idealised single linear pseudotachylyte (PST) fault vein with typical geometry of injection veins protruding into the host rock; **(b)** Segmented fault composed of several parallel pseudotachylyte fault veins that may be linked across the stepover section, either by one segment tip or by the tips of both segments. The pseudotachylyte vein is continuous across the

linkage; **(c)** Segmented fault composed of several parallel pseudotachylyte fault veins, with extensional rhombocasm pull-aparts identifiable in the stepover. The pseudotachylyte vein is continuous across the stepover; **(d)** Parallel and closely-spaced pseudotachylyte fault veins bounding a region with internal vein networks – at least some of which are fault veins – and possibly brecciation, in which case a tabular breccia is formed; **(e)** Pseudotachylyte fault vein which splits into two branches, which may display different vein thicknesses. Both branches should have accommodated shear displacement and PST injection veins or brecciation may be associated with the branches.

Figure 3. Typical microscopic features of GSZ pseudotachylytes: **(a)** optical micrograph of branching pseudotachylyte vein with high angle injection and side-wall shortcut removing curve in the vein (plane polarised light) sampled from [57.7008°N 05.6308°W]; **(b)** optical micrograph of pseudotachylyte matrix illustrating banded variation in crystal morphology (plane polarised light) sampled from [57.7066°N 05.6173°W]; **(c)** back scattered electron image of pseudotachylyte crystalline matrix capturing heterogeneous hornblende nucleation around a plagioclase clast, sampled from [57.7066°N 05.6173°W]; **(d)** back scattered electron image of pseudotachylyte matrix with radiating dendritic and microlitic hornblende, sampled from [57.7066°N 05.6173°W]; **(e)** optical micrograph of deformed hornblende clasts in pseudotachylyte (plane polarised light), sampled from [57.7008°N 05.6308°W]; **(f)** optical micrograph of deformed hornblende in intersection of injection and fault veins (plane polarised light), sampled from [57.7008°N 05.6308°W].

Figure 4. Stepped pseudotachylyte fault vein following amphibolite foliation [57.6959°N 05.6161°W]; **(a)** In the field, the fault vein (emphasised by orange shading) shows lateral steps (one indicated by arrowhead). The pseudotachylyte thickness along the fault varies from 3 - 15 mm, hammer length is 30 cm. Image shows a horizontal surface. An unannotated version of this image is available as Supplementary Figure 1; **(b)** fresh cut surface of grey pseudotachylyte fault veins with chilled margins sampled from the locality shown in Fig. 4a. White box shows location of Fig. 4c; **(c)** optical

micrograph of a stepover section with one overstep linked by only one segment (far right) and one preserved in the process of linkage involving both fault segment tips (centre) which curve towards the adjacent segment. A band of cataclasite, indicated by white arrowheads, is parallel to and partially overprinted by a pseudotachylyte segment (plane polarised light); **(d)** and **(e)** micrographs showing detail of ductile shear zones propagating in front of fault tips forming a process zone (plane polarised light).

Figure 5. Field-scale geometries of pseudotachylyte (PST) faults in GSZ amphibolites. All photos have PST traced in orange – unannotated versions are available in supplementary figure 2: **(a)** pull-apart rhombochasm forms dilational stepover within pseudotachylyte fault cutting quartz vein in amphibolite (pencil length 15 cm) [57.7007°N 05.6173°W]; **(b)** reactivation of pre-existing shear band, with pseudotachylyte lining boundary (white lines) and internal (blue lines) faults as well as injecting into foliation and locally developing into pseudotachylyte breccias. Horizontal plane of exposure [57.7121°N 05.6228°W]; **(c)** reactivation of shear bands by brittle, pseudotachylyte-bearing faults, with breccia extensively developed in the underlying band. Horizontal plane of exposure [57.7668°N 05.6168°W]; **(d)** large pseudotachylyte fault branching at its tip. Vertical plane of exposure [57.7007°N 05.6304°W]; **(e)** branching pseudotachylyte fault with injection veins developed off the thicker branch. Horizontal plane of exposure [57.6904°N 05.6066°W]; (**f**) angular, wedge-shaped breccia developed between two non-parallel faults, potentially part of a paired fault zone. Horizontal plane of exposure [57.7070°N 05.6219°W].

Figure 6. Microscale geometries of pseudotachylyte veins in optical micrographs: **(a)** millimetre scale steps in pseudotachylyte vein margin (plane polarised light) sampled from [57.7695°N 05.6132°W]; **(b)** millimetre scale steps in vein margin with additional grain-scale roughness indicated by arrowheads (plane polarised light) sampled from [57.7066°N 05.6173°W]; **(c)** ragged edge of polycrystalline clast indicates partial melting (plane polarised light) sampled from [57.7695°N 05.6132°W]; **(d)** partially melted polycrystalline clast with amphibole replaced by pseudotachylyte

and quartz and plagioclase preserved (cross polarised light) sampled from [57.7066°N 05.6173°W]; **(e)** short and blunt-ended injection veins (cross-polarised light) sampled from [57.7007°N 05.6304°W]; **(f)** blunt-ended injection vein with thin extensions (plane polarised light) sampled from [57.7008°N 05.6308°W]; **(g)** margin of pseudotachylyte vein where sidewall shortcut feature has straightened margin by removing a step. New clasts are already rounded and rotated (plane polarised light), sampled from [57.7066°N 05.6173°W].

Figure 7. Estimation of shear stress and coseismic temperature change on GSZ seismic faults; **(a)** Mohr circle construction for lithostatic stress state and strike-slip fault regime; **(b)** range of minimum seismic displacement necessary to produce thickness of 5 mm pseudotachylyte along a fault slipping at different depths in the crust. Equivalent moment magnitudes (M_W) are indicated for faults with the maximum and minimum estimated lengths of 100 m and 1 m respectively.

Figure 8. Models of formation of stepping ruptures and dilational sites through a single episode of seismic slip; **(a)** linkage of pseudotachylyte-bearing rupture segments in the 'dilational crack' style; **(b)** linkage of rupture segments via secondary faults forming dilatational pull-aparts in extensional stepovers; **(c)** Formation of elongate tabular breccias via paired ruptures and internal faults, here exploiting a shear band structure.

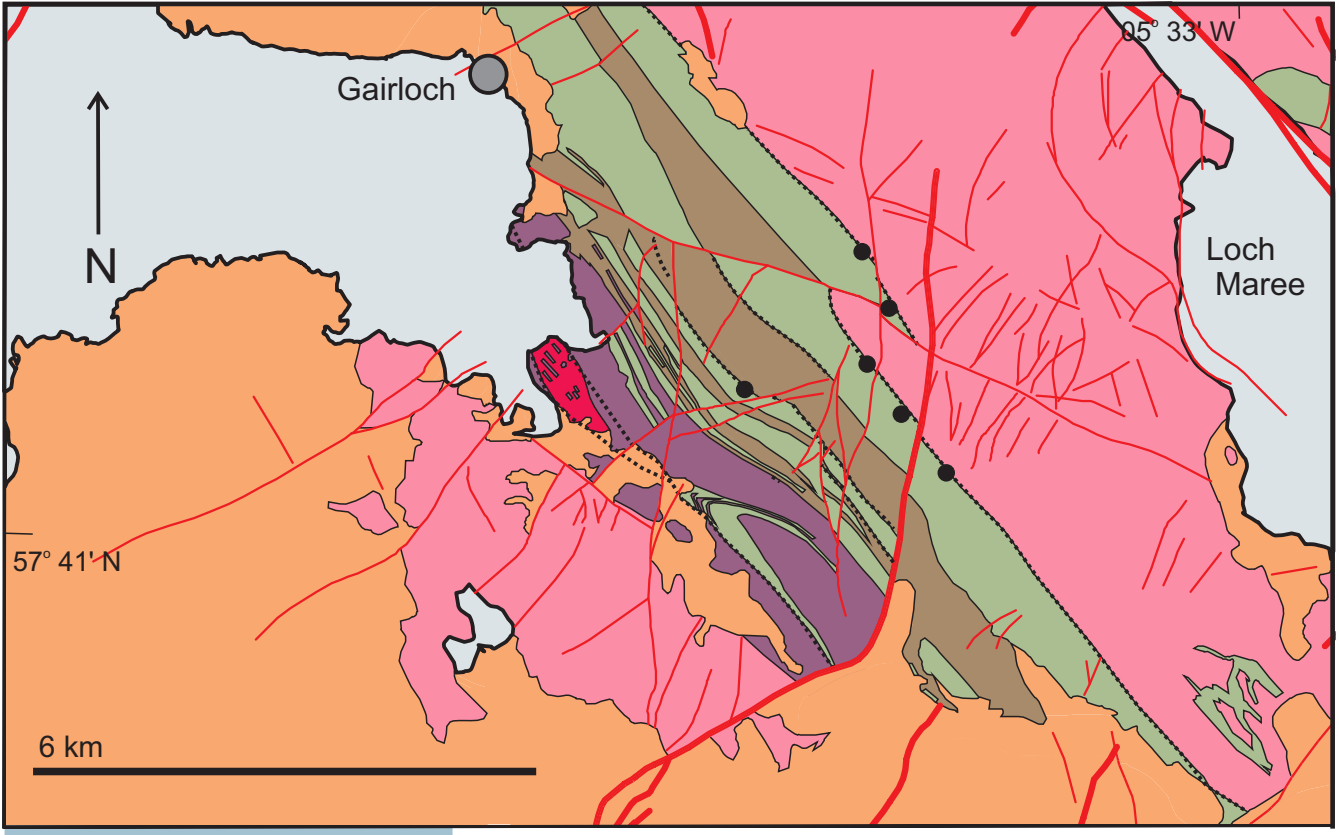

Neoproterozoic sediments

Torridon Group

Palaeoproterozoic supracrustals (Loch Maree Group)

Metasedimentary rocks, predominantly metapelite

Amphibolite

Reworked granodiorite-tonalite gneiss

Archean gneiss

Hornblende gneiss

Undifferentiated Lewisian orthogneiss (with amphibolite dykes)

Crush Belt (after Park, 1961)

Pseudotachylyte in amphibolite

Large fault

Local faults

(a)

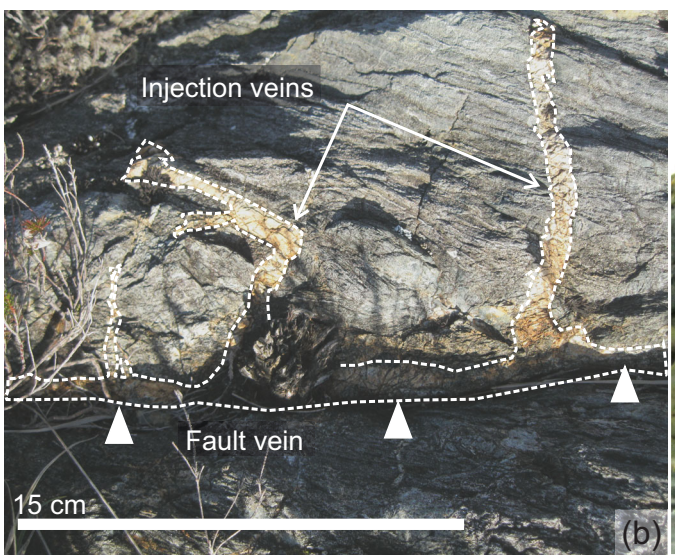

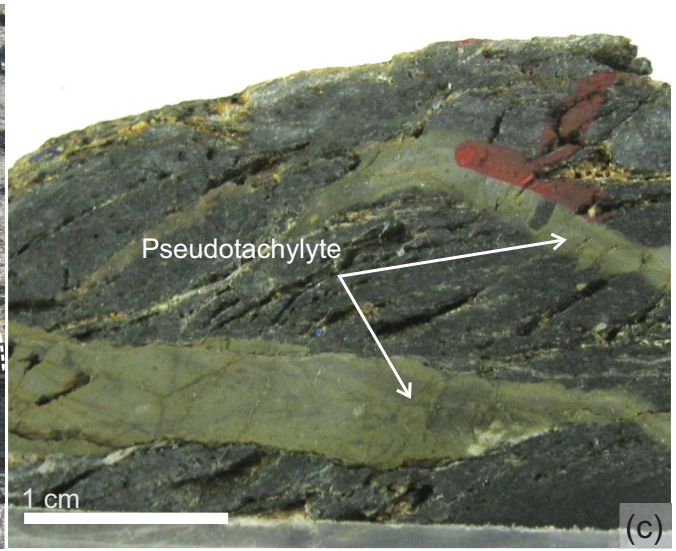

(a) Single fault vein with injection veins

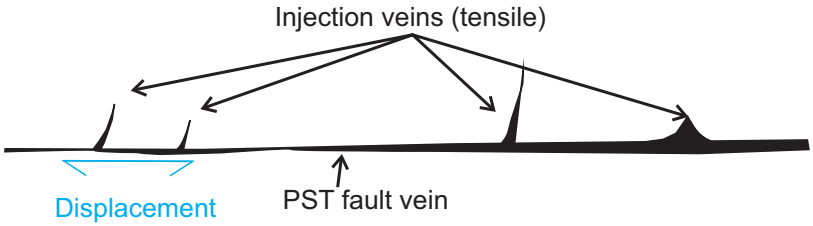

(b) Segmented fault veins with linkage

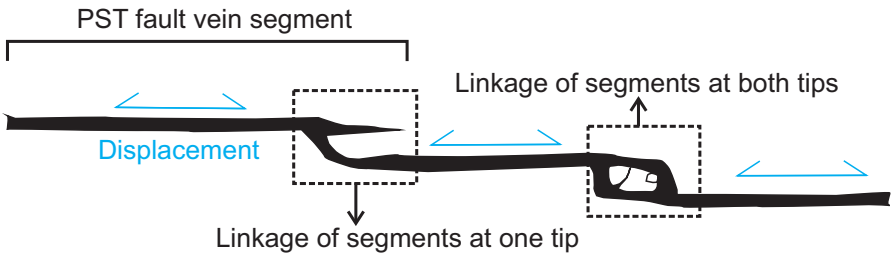

(c) Segmented fault veins with pull-aparts

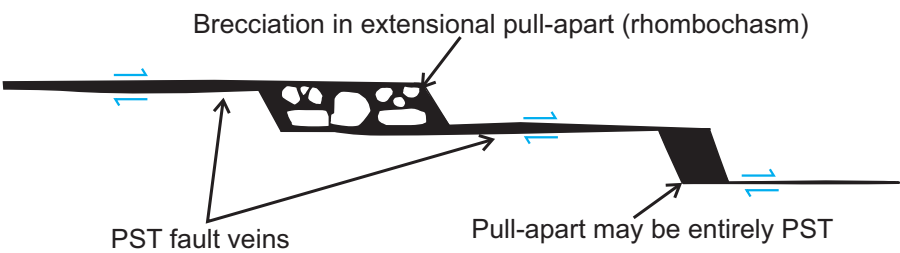

(d) Paired fault veins with internal PST networks

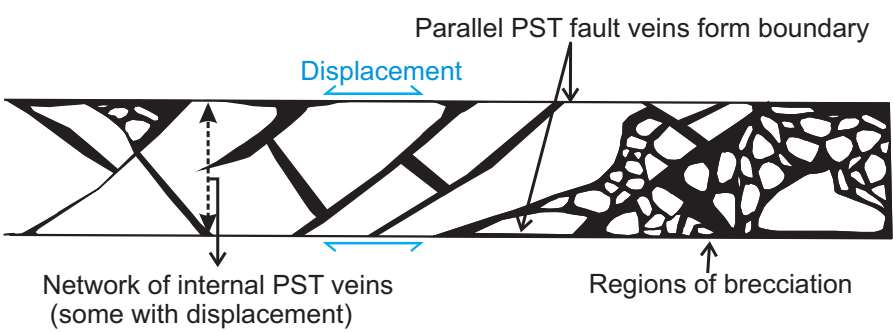

(e) Branching fault vein

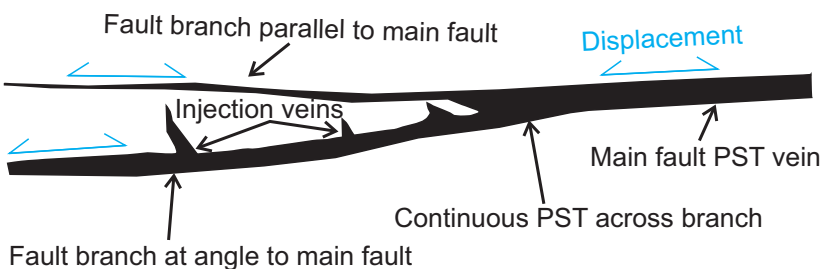

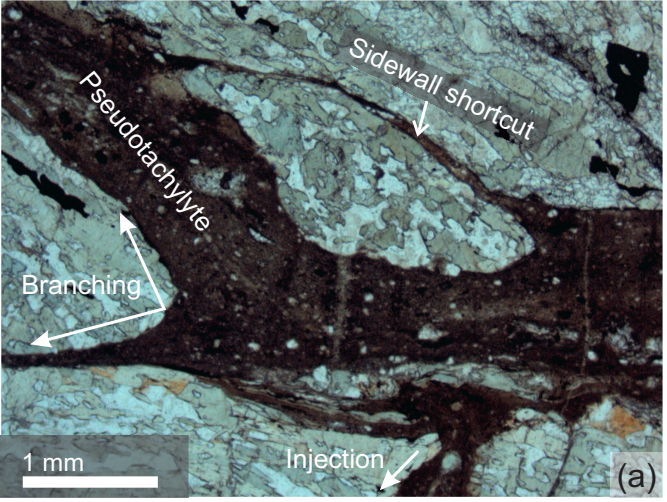
Sidewall shortcut
Pseudotachylyte
Branching
1 mm
Injection
(a)

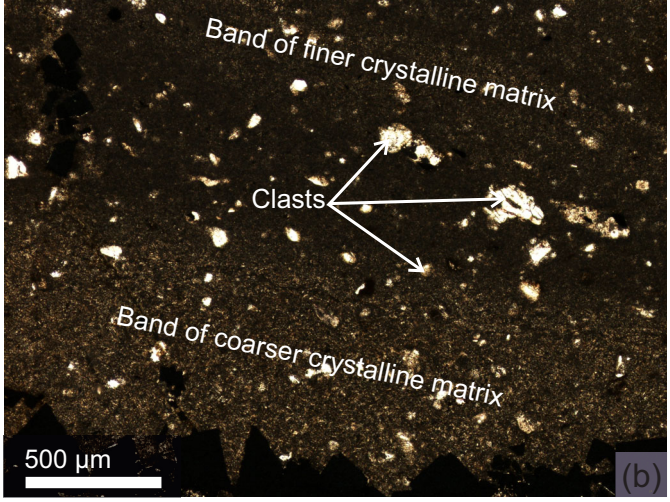
Band of finer crystalline matrix
Clasts
Band of coarser crystalline matrix
500 µm
(b)

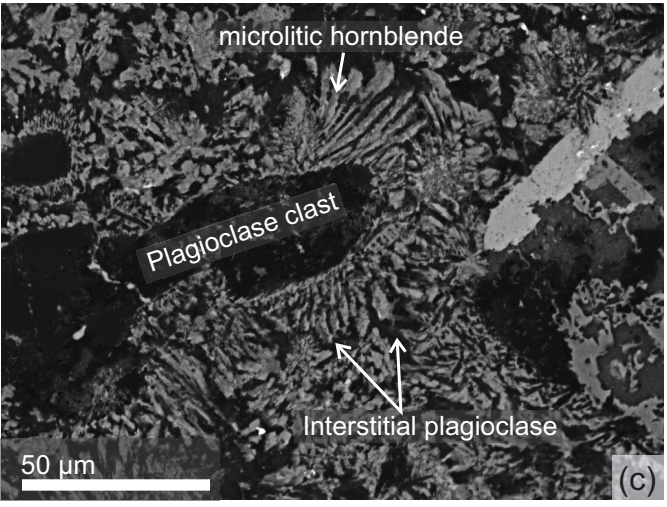
microlitic hornblende
Plagioclase clast
Interstitial plagioclase
50 µm
(c)

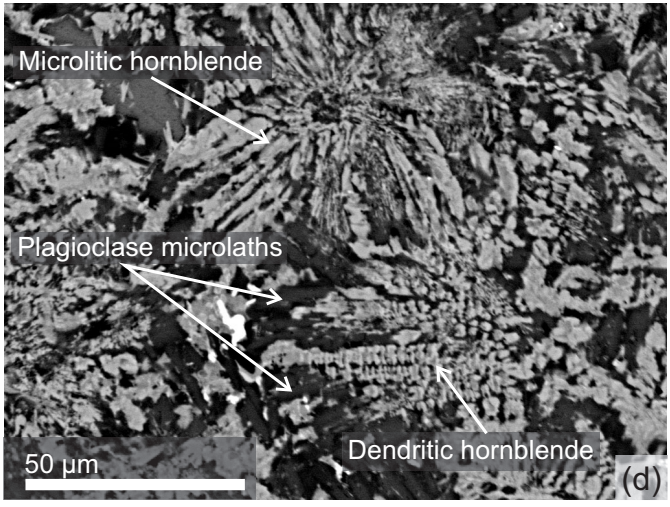
Microlitic hornblende
Plagioclase microlaths
Dendritic hornblende
50 µm
(d)

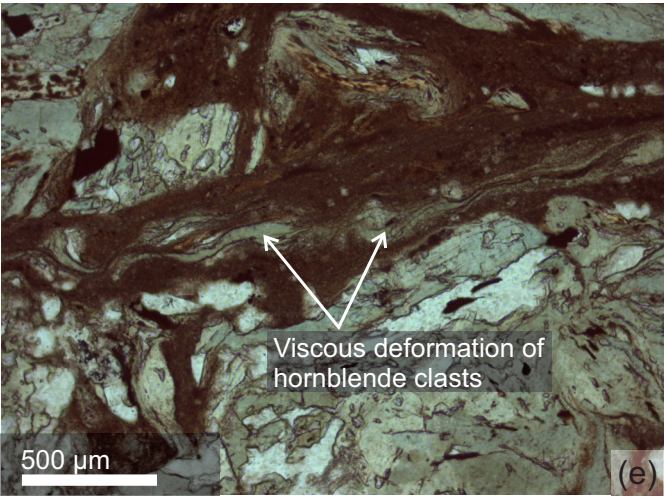
Viscous deformation of
hornblende clasts
500 µm
(e)

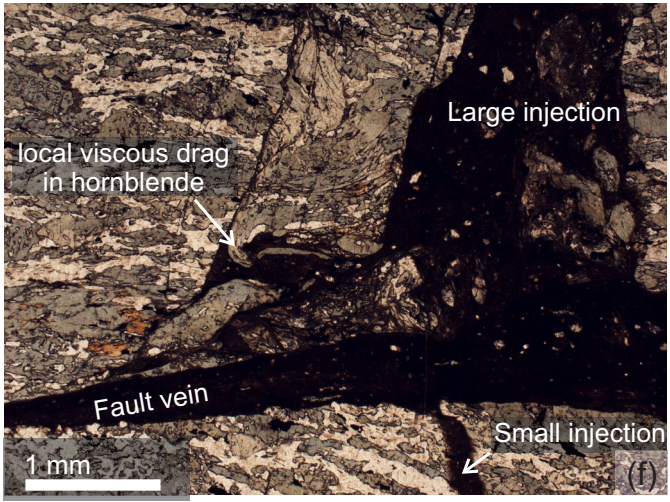
Large injection
local viscous drag
in hornblende
Fault vein
Small injection
1 mm
(f)


Pseudotachylyte fault vein
Step
Amphibolite foliation
(a)

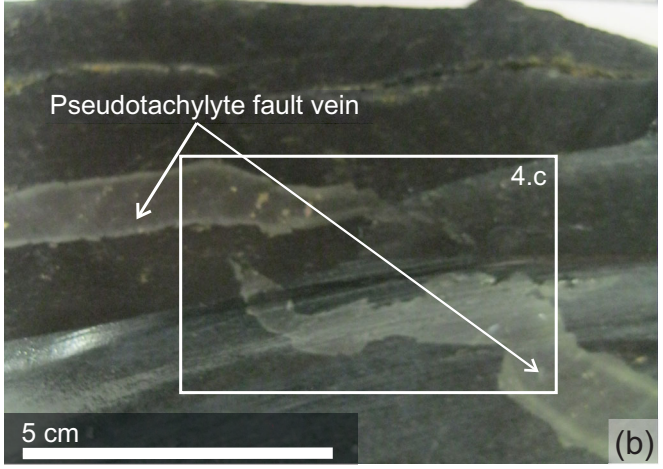
Pseudotachylyte fault vein
4.c
5 cm
(b)

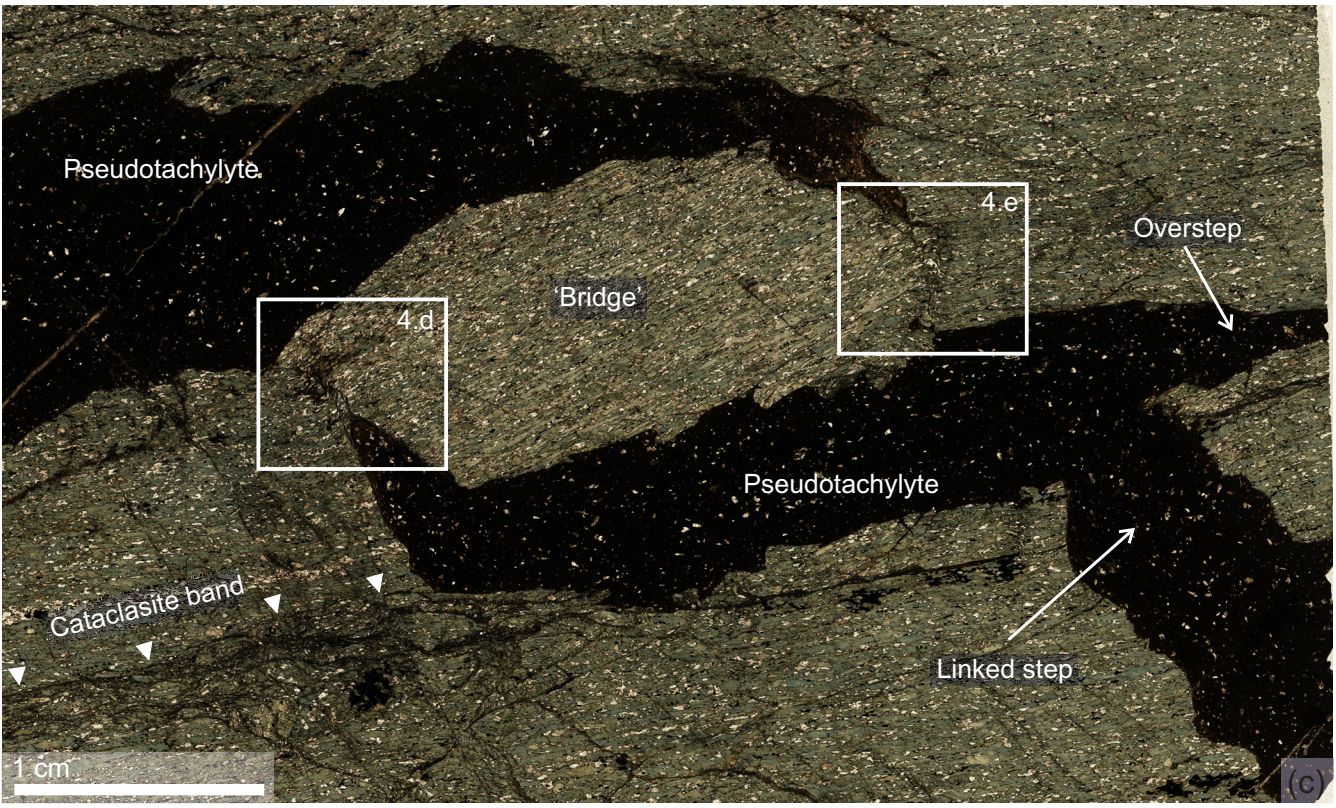
Pseudotachylyte
4.e
Overstep
'Bridge'
4.d
Pseudotachylyte
Cataclasite band
Linked step
1 cm
(c)

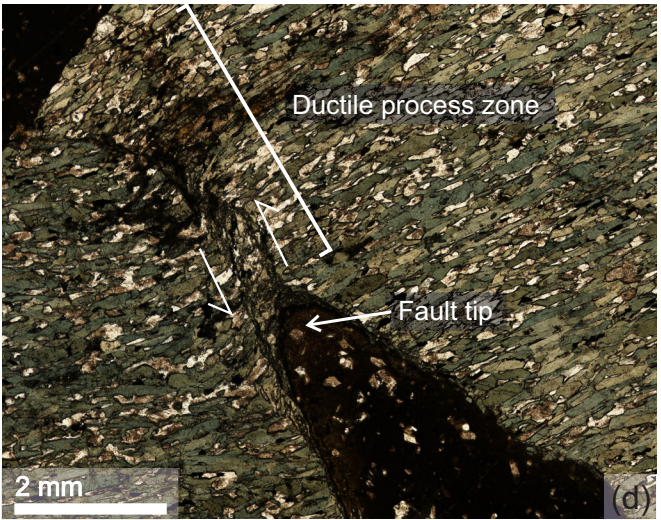
Ductile process zone
Fault tip
2 mm
(d)

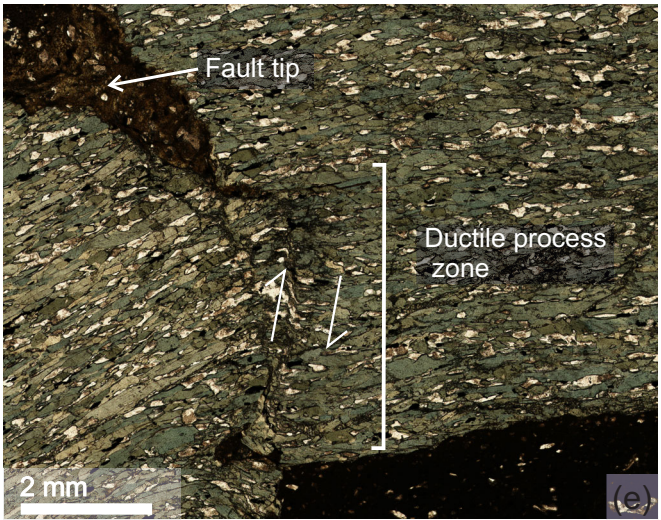
Fault tip
Ductile process zone
2 mm
(e)

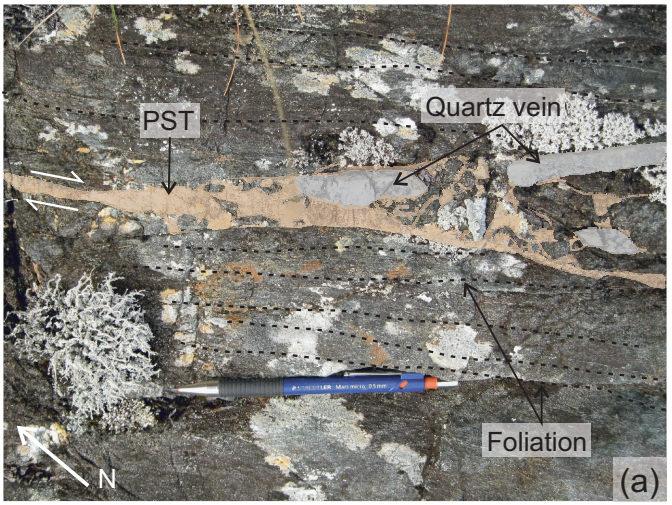
PST
Quartz vein
Foliation
N
(a)

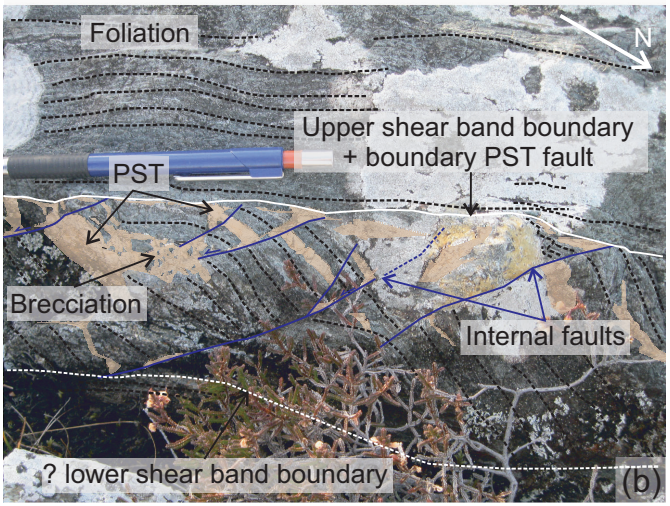
Foliation
N
Upper shear band boundary
+ boundary PST fault
PST
Brecciation
Internal faults
? lower shear band boundary
(b)

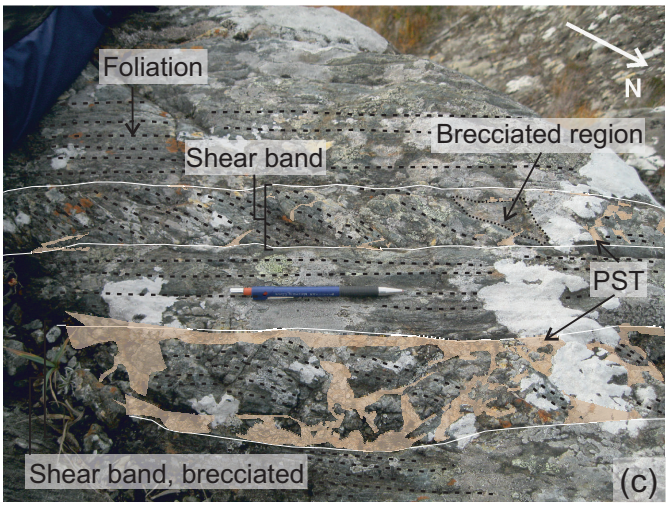
Foliation
N
Brecciated region
Shear band
PST
Shear band, brecciated
(c)

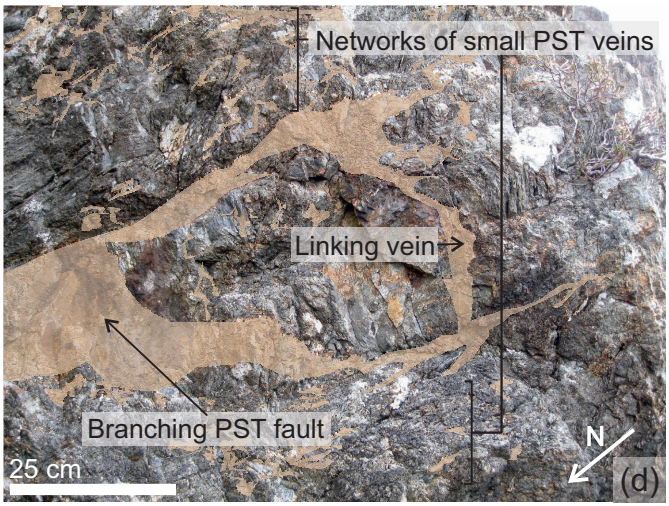
Networks of small PST veins
Linking vein
Branching PST fault
25 cm
N
(d)

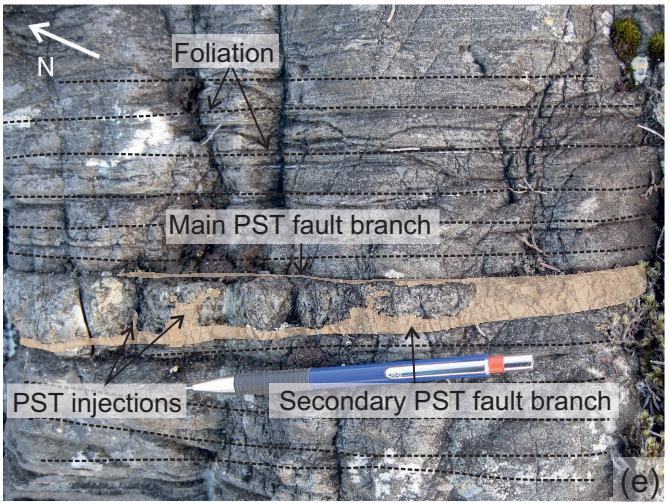
N
Foliation
Main PST fault branch
PST injections
Secondary PST fault branch
(e)

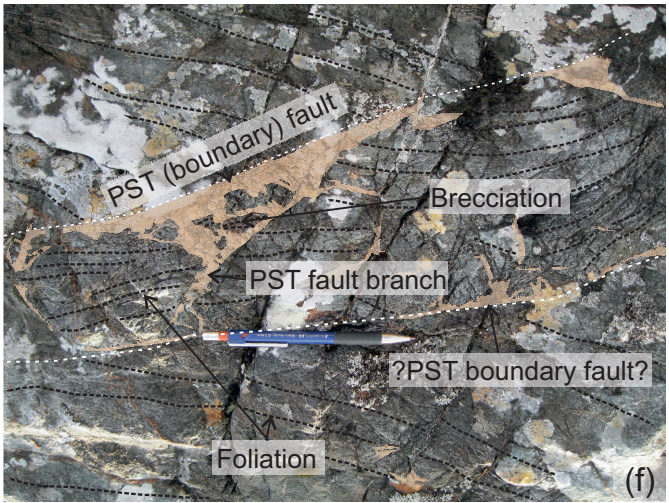
PST (boundary) fault
Brecciation
PST fault branch
?PST boundary fault?
Foliation
(f)

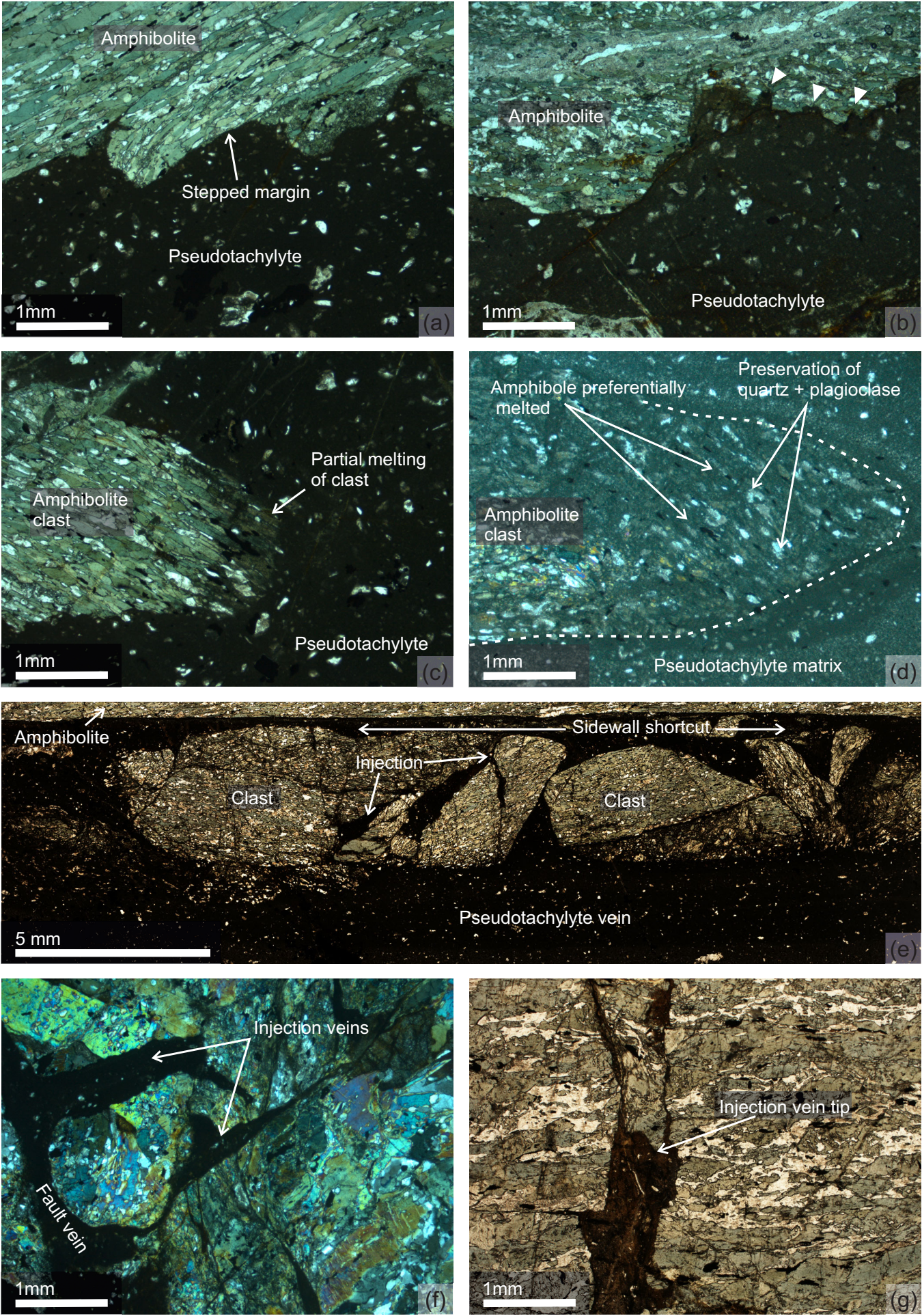
Amphibolite
Stepped margin
Pseudotachylyte
1mm
(a)
Amphibolite
Pseudotachylyte
1mm
(b)
Partial melting
of clast
Amphibolite
clast
Pseudotachylyte
1mm
(c)
Amphibole preferentially
melted
Preservation of
quartz + plagioclase
Amphibolite
clast
1mm
Pseudotachylyte matrix
(d)
Amphibolite
Sidewall shortcut
Injection
Clast
Clast
Pseudotachylyte vein
5 mm
(e)
Injection veins
Fault vein
1mm
(f)
Injection vein tip
1mm
(g)

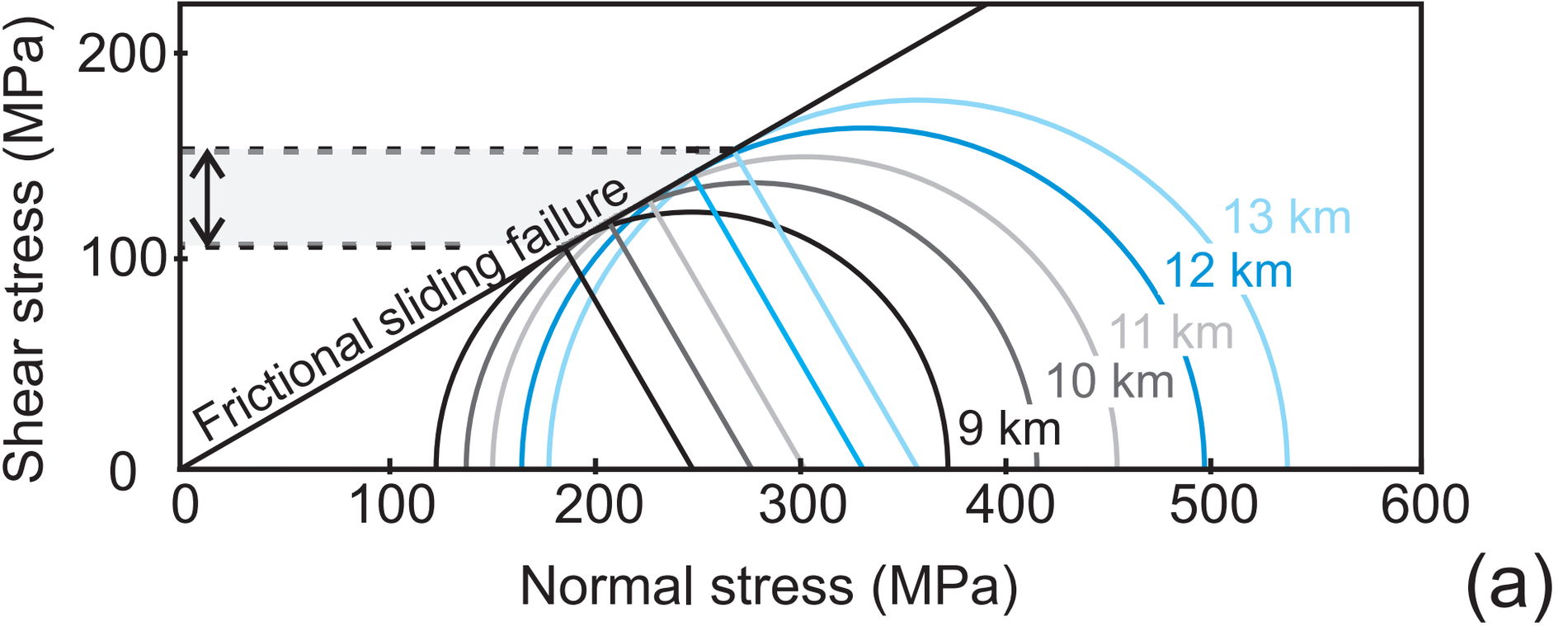
Shear stress (MPa)
200
100
0
Frictional sliding failure
13 km
12 km
11 km
10 km
9 km
0
100
200
300
400
500
600
Normal stress (MPa)

(a)

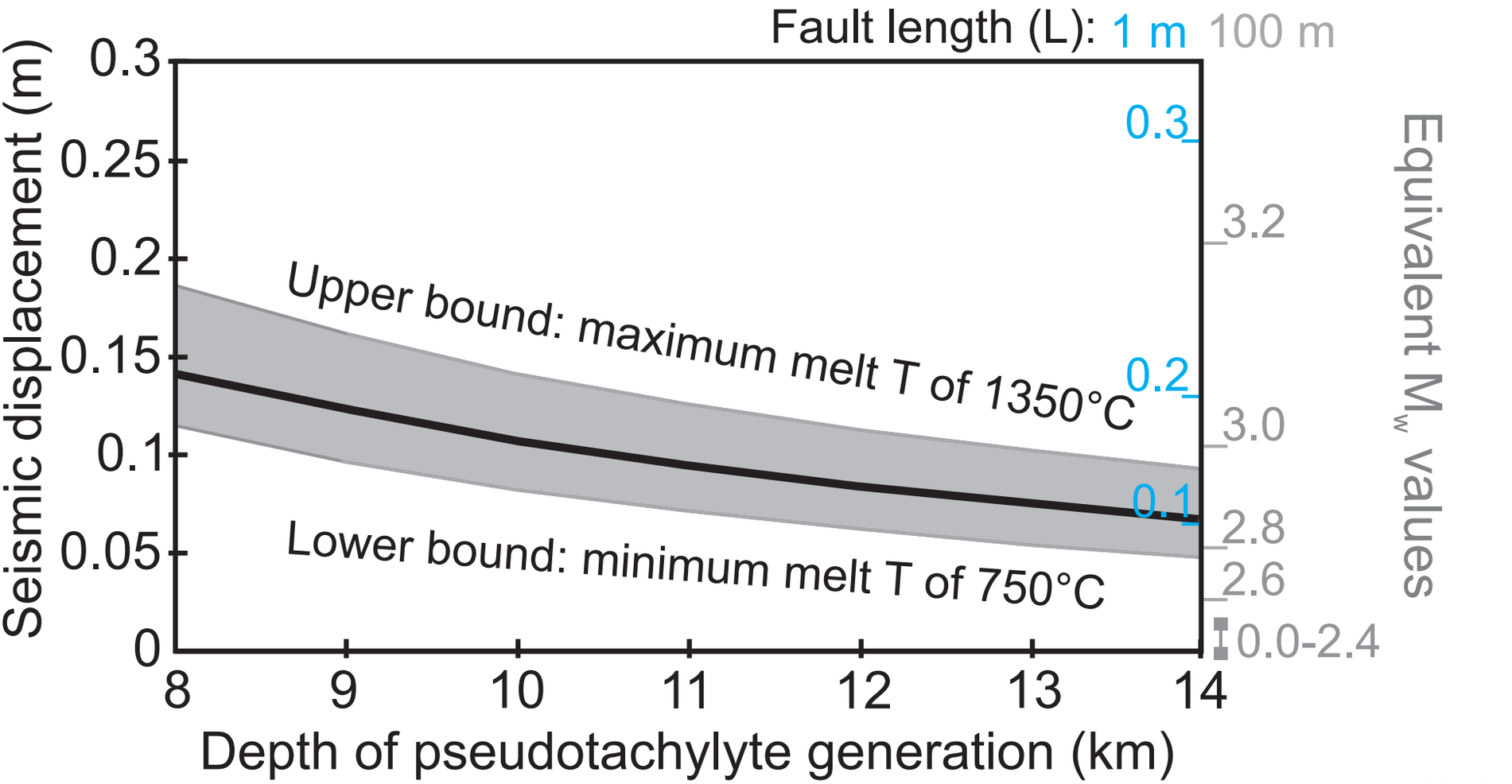
Fault length (L): 1 m 100 m
Seismic displacement (m)
0.3
0.25
0.2
0.15
0.1
0.05
0
Upper bound: maximum melt T of 1350°C
Lower bound: minimum melt T of 750°C
0.3
0.2
0.1
3.2
3.0
2.8
2.6
0.0-2.4
Equivalent M_w values
8
9
10
11
12
13
14
Depth of pseudotachylyte generation (km)

(b)

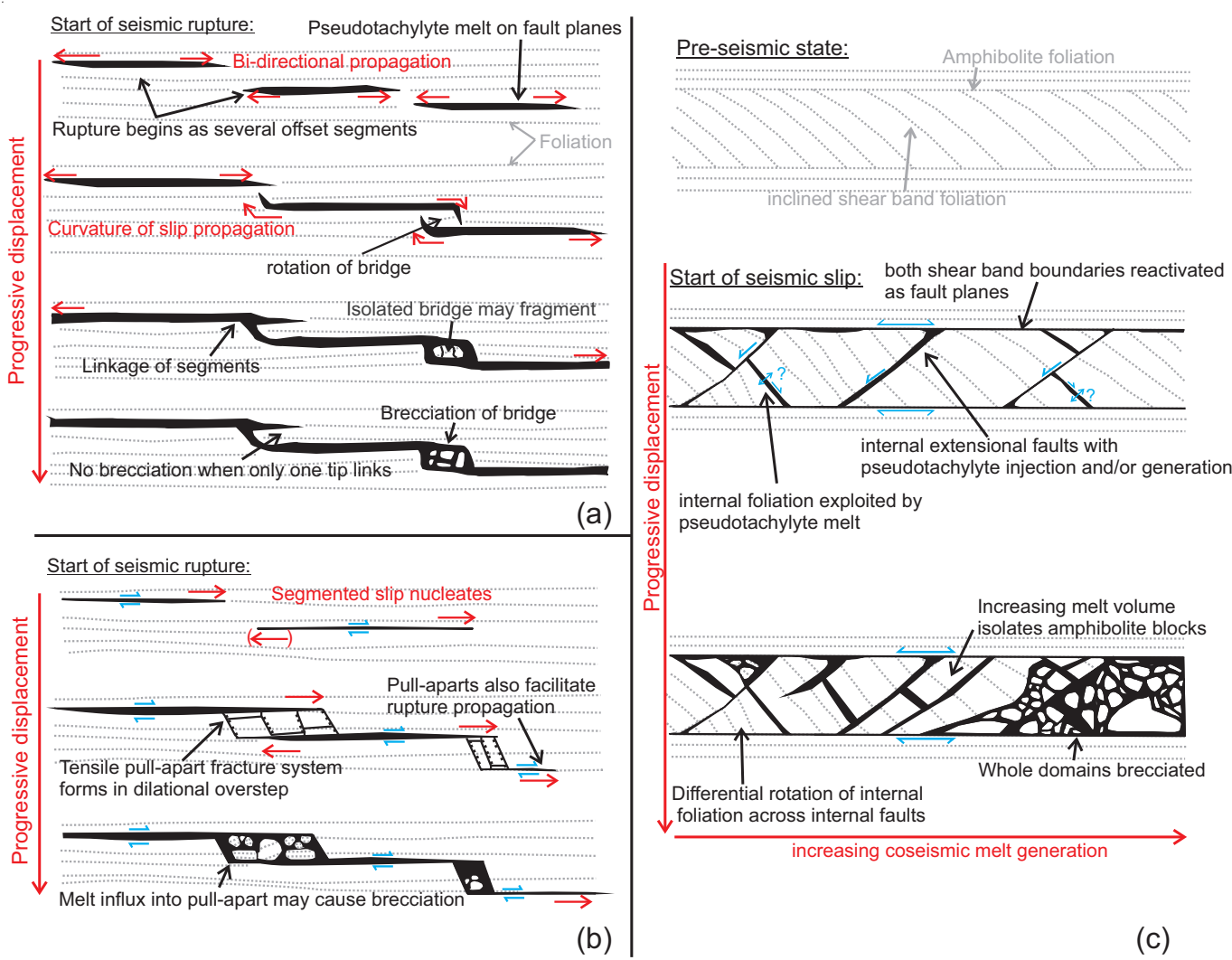
Start of seismic rupture:
Pseudotachylyte melt on fault planes
Bi-directional propagation
Rupture begins as several offset segments
Foliation
Curvature of slip propagation
rotation of bridge
Isolated bridge may fragment
Linkage of segments
Brecciation of bridge
No brecciation when only one tip links
Progressive displacement
(a)
Start of seismic rupture:
Segmented slip nucleates
Pull-aparts also facilitate rupture propagation
Tensile pull-apart fracture system forms in dilational overstep
Melt influx into pull-apart may cause brecciation
Progressive displacement
(b)
Pre-seismic state:
Amphibolite foliation
inclined shear band foliation
Start of seismic slip:
both shear band boundaries reactivated as fault planes
internal extensional faults with pseudotachylyte injection and/or generation
internal foliation exploited by pseudotachylyte melt
Increasing melt volume isolates amphibolite blocks
Whole domains brecciated
Differential rotation of internal foliation across internal faults
Progressive displacement
increasing coseismic melt generation
(c)